



HAL
open science

Discerning dominant temporal patterns of bio-optical properties in the northwestern Mediterranean Sea (BOUSSOLE site)

Marco Bellacicco, V. Vellucci, F. d'Ortenzio, David Antoine

► **To cite this version:**

Marco Bellacicco, V. Vellucci, F. d'Ortenzio, David Antoine. Discerning dominant temporal patterns of bio-optical properties in the northwestern Mediterranean Sea (BOUSSOLE site). Deep Sea Research Part I: Oceanographic Research Papers, 2019, 148, pp.12-24. 10.1016/j.dsr.2019.04.006 . hal-02374488

HAL Id: hal-02374488

<https://hal.sorbonne-universite.fr/hal-02374488>

Submitted on 15 Feb 2021

HAL is a multi-disciplinary open access archive for the deposit and dissemination of scientific research documents, whether they are published or not. The documents may come from teaching and research institutions in France or abroad, or from public or private research centers.

L'archive ouverte pluridisciplinaire **HAL**, est destinée au dépôt et à la diffusion de documents scientifiques de niveau recherche, publiés ou non, émanant des établissements d'enseignement et de recherche français ou étrangers, des laboratoires publics ou privés.

1 Discerning dominant temporal patterns of bio-optical properties in 2 the northwestern Mediterranean Sea (BOUSSOLE site)

3 Bellacicco, M.^{1*}, Vellucci, V.², D'Ortenzio, F.¹, Antoine, D.^{1,3}

4
5 ¹Sorbonne Université, CNRS, Laboratoire d'Océanographie de Villefranche, LOV, F-06230 Villefranche-
6 sur-Mer, France

7 ²Sorbonne Université, CNRS, Institut de la Mer de Villefranche, IMEV, F-06230 Villefranche-sur-Mer,
8 France

9 ³Remote Sensing and Satellite Research Group, School of Earth and Planetary Sciences, Curtin University,
10 Perth, WA 6845, Australia

11
12 *Corresponding author e-mail: Marco.Bellacicco@obs-vlfr.fr

13
14 **Keywords:** phenology, bio-optical properties, time-series analysis, wavelet analysis

15 16 **Highlights:**

- 17
- 18 • The Chl-Fluo variability has driven mostly by annual cycle.
- 19 • The c_p and b_{bp} coefficients have driven mostly by 6-months cycle.
- 20 • During winter, mid-term cycles (greater than 10 days) dominate the intra-seasonal signal for all
21 parameters.
- 22 • During summer, diel cycle has a strong impact on the intra-seasonal variability for all parameters.

23 24 **Abstract**

25
26 A wavelet analysis has been applied, for the first time, to 3-year high-frequency field observations
27 of bio-optical properties (*i.e.* chlorophyll-fluorescence, beam attenuation and backscattering
28 coefficients) in the northwestern Mediterranean Sea (BOUSSOLE site), in order to identify their
29 dominant temporal patterns and evolution. A cross-wavelet and coherence analysis has also been
30 applied to paired bio-optical coefficients time-series at the BOUSSOLE site, which allows
31 identifying the temporal relationship between the cycles of the bio-optical properties. Annual, six-
32 and four- month, intra-seasonal (*i.e.*, mid- and short-terms) cycles are identified from the time-
33 series analysis. The periodicities of chlorophyll-fluorescence, beam attenuation and particulate
34 backscattering coefficients correlate well at different temporal scales and specific seasons. At
35 annual, six- and four- month scales, different bio-optical properties follow rather similar patterns,
36 likely driven by physical forcing. Intra-seasonal variability consists in both mid- and short-term
37 variations. The former dominates during the winter and are related to episodic bloom events, while
38 the latter variations (*i.e.*, diel) prevail during summer, in a stratified water column.

39 1. Introduction

40 Phenology is the study of the timing of periodic life events (*Morren*, 1849a; *Winder et al.*, 2010). It
41 was first investigated on terrestrial plants, which are sensitive to climate variability (*Cleland et al.*,
42 2007; *Winder et al.*, 2010). Phenology of marine ecosystems has been studied for a few decades,
43 especially by use of bio-optical proxies that are accessible through satellite ocean color remote
44 sensing. In the ocean, phytoplankton are considered as a sentinel of changes in the ecosystems,
45 because they respond rapidly to environmental perturbations (*Bode et al.*, 2015). In such a context,
46 several studies on phytoplankton phenology (*i.e.* seasonal and annual cycles) have been conducted
47 in marine ecosystems, from inland to open ocean waters, using chlorophyll-*a* data (*Behrenfeld et al.*
48 2010, 2016; *Winder et al.* 2010; *Carey et al.* 2016; *Mignot et al.*, 2018). Other cycles (*e.g.* lowest
49 temporal cycles) are less well-known.

50 In the ocean, changes in nutrients and light conditions have an impact on the phytoplankton
51 standing stock and on the intracellular chlorophyll concentration (Chl), which is widely used as a
52 proxy for phytoplankton biomass (*Volpe et al.*, 2012; *Siegel et al.*, 2013). In the Mediterranean Sea,
53 under high nutrients and low light, phytoplankton growth rate shows the maximum concentration
54 values. When light intensity increases, there is no longer a need for the cells to produce and sustain
55 large amounts of the energetically expensive chlorophyll pigment. Under these conditions,
56 phytoplankton exploit the nutrients still present in the upper layer. This, together with the light
57 conditions provided by the increased stratification, allows phytoplankton to grow, despite
58 phytoplankton chlorophyll concentration decreases. The condition of the strong increase in light
59 determines the decline of phytoplankton pigment demand, while low nutrient concentrations limit
60 phytoplankton population growth and division rates. Under low nutrients (generally the period of
61 highest stratification of water column) and high light conditions, phytoplankton shows the minima
62 of abundance. When light starts to decrease and mixing occurs again, phytoplankton assign the
63 energy from the newly available nutrients into the production of chlorophyll, however, limiting
64 their growth rate (*Lavigne et al.*, 2013; *Bellacicco et al.* 2016; *Barbieux et al.*, 2018).

65 In temperate seas like the Mediterranean Sea, a major feature of the annual cycle is the spring
66 bloom, as it occurs, for instance, in the Gulf of Lion (*D'Ortenzio et al.*, 2014; *Mayot et al.*, 2017).
67 This bloom typically persists for a few weeks to months. The variability of phytoplankton annual
68 and seasonal patterns has thus been well studied (*Behrenfeld et al.* 2010; *Volpe et al.*, 2012;
69 *Lavigne et al.*, 2013, *Mignot et al.*, 2014), while no systematic analyses at shorter time scales have
70 been conducted to identify the characteristic periods of biomass variability and recurrence along
71 years at these scales. *Winder et al.* (2010) defined the mid- and low-term phytoplankton fluctuations
72 as irregular blooms that are often responses to short-term weather events which affect sea
73 temperature and vertical mixing dynamics. However, several works have shown that Chl can be
74 complemented with other parameters to describe the ocean ecosystem complexity and
75 phytoplankton dynamics (*Behrenfeld et al.* 2005, 2006; *Ji et al.*, 2010). These works demonstrated
76 that the physiological processes affect the carbon to chlorophyll ratio (*Halsey and Jones*, 2015),
77 especially during intermediate periods of light and nutrients variations, as it occurs in the
78 Mediterranean Sea (*Bellacicco et al.*, 2016). Furthermore, biological processes such as
79 phytoplankton photosynthesis and cellular growth and division can be associated with short-term
80 temporal variations like the daily light-dark cycle (*Neveux et al.*, 2003; *Poulin et al.*, 2018). Diel
81 variability is often not taken into account in the current ocean colour algorithms, but many
82 laboratory experiments and studies have demonstrated that, in seawater, there is a diurnal variation

83 of optical properties, from midday to night, that have implications on biomass measurements
84 (Poulin *et al.*, 2018). Thus, the use of other proxies, such as optical coefficients, may be helpful to
85 investigate the different temporal scales of phytoplankton avoiding to take into account the effect of
86 physiological processes on Chl content. In such a context, bio-optical relationships have been
87 widely established between inherent optical properties (IOPs) and the main biogeochemical
88 parameters, such as the Chl concentration or fluorescence (Huot *et al.*, 2007, 2008; Dall'Olmo *et*
89 *al.*, 2009, 2012; Brewin *et al.*, 2012; Antoine *et al.* 2011; Martinez-Vicente *et al.*, 2013; Barbieux *et*
90 *al.*, 2018; Bellacicco *et al.*, 2018).

91 One of the most studied IOPs is the particulate beam attenuation coefficient, c_p , used as a proxy for
92 particle concentration and sensitive to a size range that includes phytoplankton cells (Claustre *et al.*,
93 1999; Behrenfeld and Boss, 2003). c_p is the sum of particulate scattering and absorption
94 coefficients. Its diel variation is primarily due to planktonic adaptation to the daily light cycle, the
95 dynamics of the upper mixed layer and the variations of particles mass (Siegel *et al.*, 1989; Walsh *et*
96 *al.*, 1995; Stramski and Reynolds, 1993; Durand and Olson, 1998). The interpretation of diel
97 variability of c_p is difficult because it depends on several factors, such as: i) phytoplankton
98 concentration and composition, ii) physiological status (*i.e.* photoacclimation), and iii)
99 concentrations of detritus and small heterotrophs (*e.g.* heterotrophic bacteria). The compound effect
100 of variations of these factors on c_p remains poorly known (Kheireddine *et al.*, 2014). Recently,
101 Gernez *et al.* (2011) and Kheireddine *et al.* (2014) have shown that the amplitude and phasing of c_p
102 diel cycles vary seasonally, which may result from seasonal changes in nutrient concentrations,
103 phytoplankton abundance, size distribution, and composition. Unfortunately, c_p is not directly
104 derivable from satellite observations, thus limiting its applications. The IOP that is directly
105 proportional to the ocean reflectance and can be retrieved from space is the particulate
106 backscattering coefficient, b_{bp} (Lee *et al.*, 2002). Similarly to c_p , b_{bp} is related to particle
107 concentration to the first order, whereas it also contains information on the particle size distribution,
108 refractive index, shape and structure of particles (Twardowski *et al.*, 2001, Neukermans *et al.*, 2012,
109 Slade and Boss, 2015). b_{bp} is more influenced than c_p by submicron non-algal particles (Morel and
110 Ahn, 1991; Stramski and Kiefer, 1991, Stramski *et al.*, 2004), yet their magnitude both covary with
111 phytoplankton concentration, allowing relationships between b_{bp} and Chl to be observed (Bellacicco
112 *et al.*, 2016, 2018; Barbieux *et al.*, 2018). Organelli *et al.*, (2018) suggest that most of b_{bp} signal is
113 due to particles with equivalent diameters between 1 and 10 μm , and thus may be significantly
114 influenced by phytoplankton. Several studies have shown good relationships between both the
115 optical coefficients and phytoplankton in terms of Chl, carbon or fluorescence, on both global and
116 regional scales (Behrenfeld and Boss, 2003; Behrenfeld *et al.*, 2005; Dall'Olmo *et al.*, 2009, 2012;
117 Antoine *et al.*, 2011; Brewin *et al.*, 2012; Martinez-Vicente *et al.*, 2013; Barbieux *et al.*, 2018;
118 Bellacicco *et al.*, 2018). The complexity of temporal relationships between c_p , b_{bp} , and
119 phytoplankton biomass proxies should be, thus, studied and observed at a range from diel to annual
120 cycles.

121 The objectives of this study are to determine the intra-annual dominant temporal patterns (from the
122 lowest up to annual cycles) of the above-mentioned bio-optical parameters, the changes of these
123 cycles over time, the characteristics and recurrence strength at those periods and to define the
124 temporal relationship between the cycles of the bio-optical properties. To this aim a Wavelet
125 Analysis (WA) was applied, for the first time, to a 3-year time-series (2011–2013) of surface Chl-
126 fluorescence, b_{bp} and c_p at the BOUSSOLE site in the northwestern (NW) Mediterranean Sea

127 (*Antoine et al.*, 2006; Figure 1), enabling the detection of all the intra-annual dominant temporal
128 patterns.

129

130 2. Area of study, data and methods

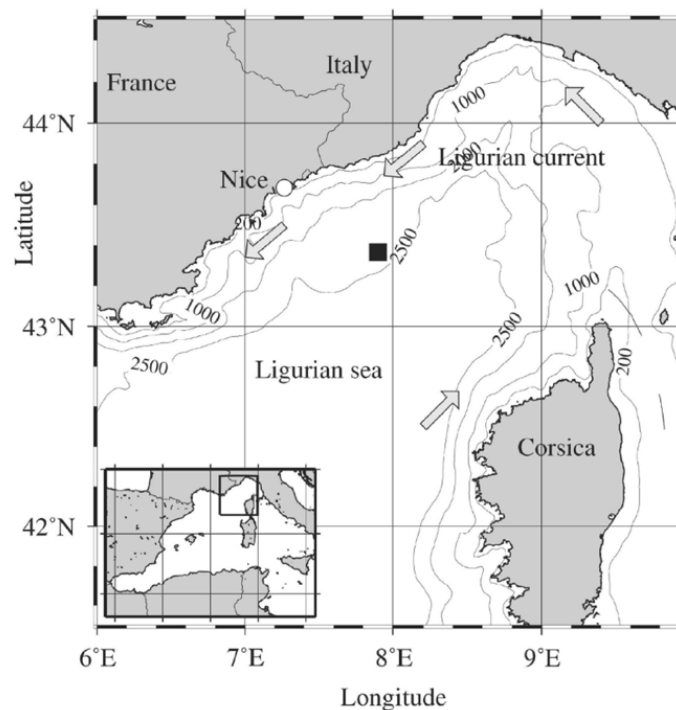
131

132 2.1 BOUSSOLE site

133 The BOUSSOLE (*BOU*ee pour l'*acqui*Sition d'une *Série* *Optique* a Long *term*E) project started in
134 1999, and its activities are developed on a site located in the northwestern Mediterranean Sea, at
135 about 32 nautical miles from the French coast (Figure 1). Essential information about the site
136 characteristics, the measurement platform, and the instrumentation are also provided in *Antoine et*
137 *al.* (2006, 2008a,b). The site is protected from coastal inputs by the Ligurian Current, which flows
138 along the coast toward the southwest (*Millot*, 1999). The physical conditions of the area show
139 strong seasonality (*D'Ortenzio et al.*, 2014), with deep (~400 m) mixed layers in winter, and a
140 marked stratification in summer (~20 m; *Antoine et al.*, 2011; *Mayot et al.*, 2017). Hydrodynamics
141 drive seasonal changes in phytoplankton abundance, which shows a typical mid-latitude temporal
142 pattern. Oligotrophic conditions prevail in summer where Chl is about 0.1 mg m⁻³ (minima ~0.05
143 mg m⁻³), and concentrations increase up to 3–5 mg m⁻³ during the spring bloom, and stay between
144 0.1–0.3 mg m⁻³ the rest of the year (*Gernez et al.*, 2011, *Kheireddine et al.*, 2014). There is,
145 accordingly, a large range of optical properties (*Antoine et al.*, 2006; *Gernez et al.*, 2011), as
146 observed over the entire northwestern Mediterranean Sea (*Bosc et al.*, 2004).

147 A moored buoy has been permanently deployed at the BOUSSOLE site since September 2003 and
148 operates in a quasi-continuous mode, with data acquisition for one minute every 15 min both night
149 and day. Adequate measures have to be taken to minimize or eliminate bio-fouling, which is
150 unavoidable with moored instrument. All instruments installed on the BOUSSOLE buoy are
151 cleaned by divers about every 2 weeks.

152



153

154 Figure 1: The area of the north-western Mediterranean Sea showing the main current branches (grey arrows),
155 and the location of the BOUSSOLE site in the Ligurian Sea (black square) (*Antoine et al.*, 2011).

156 2.2 Optical measurements

157 The volume scattering function at 140° , $\beta(140)$, is measured using in alternation two HOBI Labs
158 Hydroscat-4 backscattering meters installed at the lower measurements depth of the buoy (*ca.* 9 m).
159 Instruments are calibrated before deployments (which last about 6 to 12 months) and are equipped
160 with filters at 442, 488, 550, and 620 nm, here only the green band is used. The instruments operate
161 at 1 Hz, so that about 60 measurements are recorded during 1 minute, from which the median is
162 taken as representative for $\beta(140)$. Dark current measurements are performed on site with a
163 neoprene cap covering the instrument windows, average dark readings are subtracted to the time-
164 series for each deployment. The $\beta(140)$ values are also corrected for attenuation along the
165 measurement path (the $\sigma(\lambda)$ correction of *Maffione and Dana*, 1997) using c_p (see below) and the
166 total absorption coefficient derived from inversion of the diffuse attenuation coefficient for
167 downward irradiance (K_d) and the irradiance reflectance (R). K_d and R are retrieved from parallel
168 measurements performed with a set of Satlantic OCR-200 series radiometers. b_{bp} is derived from
169 the corrected $\beta(140)$ as follows (*Maffione and Dana* 1997; *Boss and Pegau*, 2001):

$$170 \quad b_{bp}(550) = 2\pi\chi_p(\beta(140,550) - \beta_w(140,550)) \quad (m^{-1}) \quad [1]$$

171 where $\chi_p=1.13$ (*D. R. Dana and R. A. Maffione*, unpublished manuscript, 2014) and $\beta_w(140)$, the
172 pure seawater scattering at 140° , is computed following *Zhang et al.*, (2009); *Zhang and Hu* (2009)
173 using the temperature and salinity measured at the same depth with a Sea-Bird Scientific SBE-37SI
174 CTD sensor.

175 The particulate transmittance (Tr_p , %) at 650 nm is measured at 4 and 9 m with 25 cm path length
176 WETLabs C-Star transmissometers (acceptance angle is 1.2°). Instruments are factory calibrated
177 with deionized, ultra-filtered, UV-screened water. The corresponding particulate beam attenuation
178 coefficient, c_p , is then calculated as:

$$180 \quad c_p(650) = -\frac{1}{0.25} \ln \left(\frac{Tr_p(650)}{100} \right) \quad (m^{-1}) \quad [2]$$

181 This assumes that absorption by colored dissolved organic matter (CDOM) is negligible at 650 nm
182 (*Bricaud et al.*, 1981).

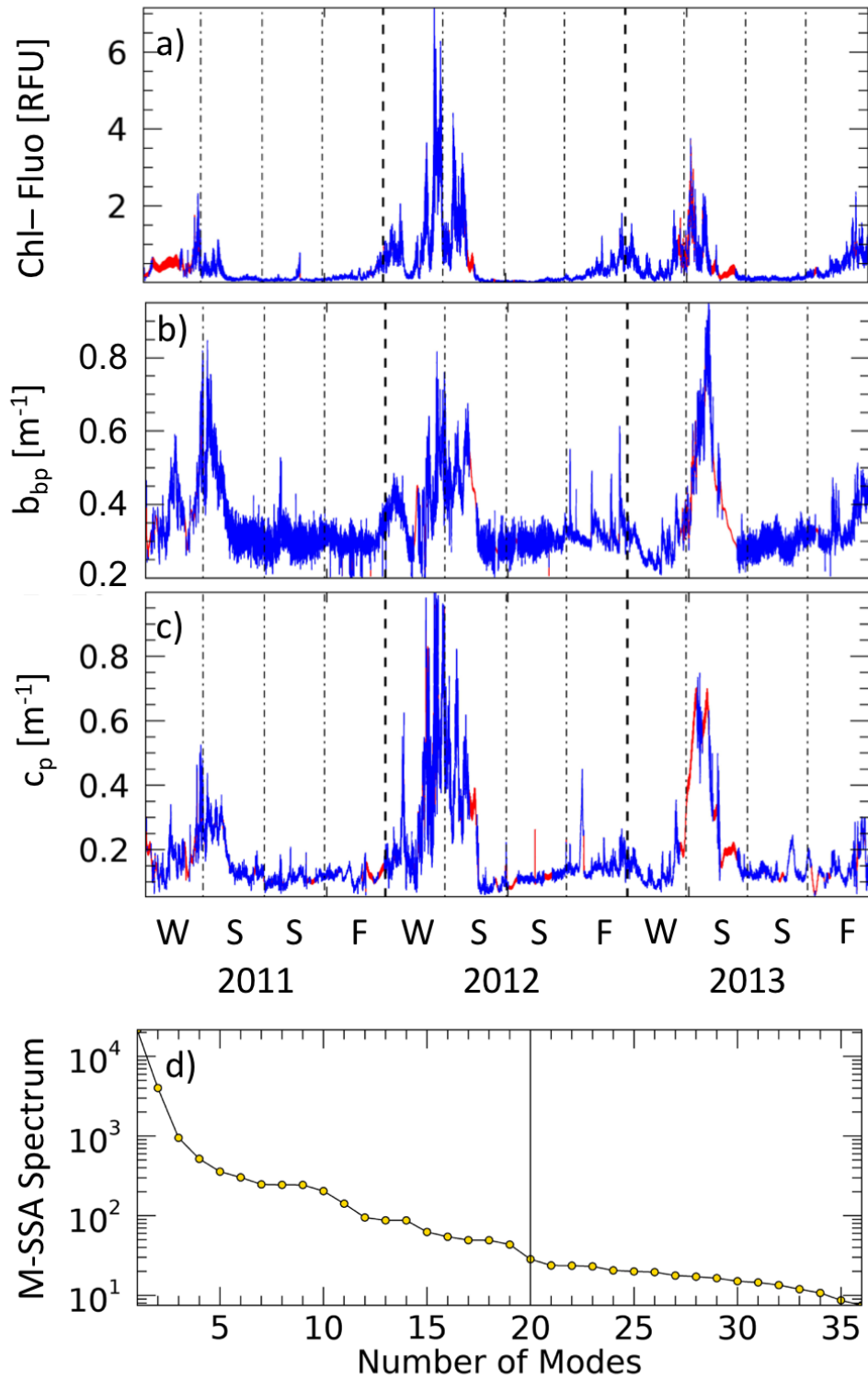
184 Chlorophyll-a fluorescence (Chl-Fluo) is measured in RFU with an ECOFLNTUs WET Labs (now
185 Sea-Bird Scientific) fluorimeter (470 nm EX/695 nm EM; see
186 <https://www.seabird.com/combination-sensors/eco-flntu/family?productCategoryId=54758054352>)
187 at 4 m and 9 m depth.

188 In this study, we selected b_{bp} , c_p and Chl Fluo at the depth of 9 m in order to compare them together.
189 Here, b_{bp} is referred to b_{bp} at 550 nm (m^{-1}), c_p to c_p at 650 nm (m^{-1}).

190 2.3 Multi-Channel Spectral Analysis (M-SSA)

191 For each parameter, the period from 2011 to 2013 was used for a total of 105216 measurements
192 after quality control (Figure 2). It consists in removing outliers using three standard deviations ($\pm 3\sigma$)
193 confidence limit.

194 An important prerequisite for applying WA is that the time-series has to be continuous at the
195 minimum considered frequency. Missing data, including those not passing quality control,
196 represented 19.57%, 13.40% and 22.38% of Chl-Fluo, b_{bp} and c_p time-series, respectively. Gaps
197 were filled using a Multi-Channel Singular Spectral Analysis (M-SSA) technique which is a non-
198 parametric spectral estimation method relying on data only (Ghil *et al.*, 2002; Kondrashov *et al.*
199 2006, 2010). This technique is not based on *a priori* parametrized family of probability distribution.
200 The method uses temporal correlation to fill in the missing data and represents a generalization of
201 the Beckers *et al.*, (2003) spatial empirical orthogonal functions-(EOFs) based reconstruction.
202 Kondrashov and Ghil (2006) demonstrated that an increased number of gaps yields the same effect
203 as an increase of the noise in the measurements. Two different inputs are required to apply M-SSA
204 for field reconstruction: window-length (W) and components (M). Both depend on the
205 characteristics of the time-series, and need to be accurately defined to avoid any bias in the
206 reconstructed fields. The W represents the length of the sliding window (expressed in number of
207 observation) used in the M-SSA in order to identify the leading components of the time-series (Ghil
208 *et al.*, 2002; Kondrashov *et al.* 2006, 2010). Diversely, M is the number of eigen-functions used for
209 signal reconstruction. Here, we applied the M-SSA to the three time-series using specific W
210 ($W=5000$) and M components (*i.e.*, $M = 1$ up to 20) following the recommendations listed in Ghil *et*
211 *al.*, (2002) and Kondrashov *et al.* (2005, 2006, 2010). These settings are compatible with the
212 properties of the time-series hereby analyzed, taking into account long, mid- and short-term
213 variations. Figure 2 (a, b, c) shows the time series of each parameter with missing data
214 reconstructed after application of M-SSA technique. Figure 2d is the M-SSA spectrum of filled
215 time-series with $W=5000$. The optimum number $M=20$ corresponds to the number of modes that
216 explain more than 95% of the variance the M-SSA spectrum.



217

218 Figure 2: Time-series of Chl-Fluo (a), b_{bp} (b), c_p (c) for 2011 – 2013 at the BOUSSOLE site. Original data
 219 are displayed with blue lines, while the gaps-filled by the M-SSA technique are highlighted with red lines.
 220 The letters W stands for winter, S for spring, S for summer and F for fall. Panel d is the M-SSA spectrum of
 221 filled time-series with the break of the slope spectrum at 20.

222

223

224 2.4 Wavelet analysis

225 Since it was first introduced by *Morlet* (1982; Part I and II), WA has been widely applied to
226 different fields of science. The main characteristic of the WA lays on the decomposition time-
227 series, and its time-scale localization and amplitude. Usually, a signal of the series can be
228 decomposed into different harmonic components using, for example, the Fourier method. This can
229 be defined as a partition of the variance of the series into its different oscillating components with
230 different frequencies (*i.e.* the periods). The spectral frequency analysis based on the widely-used
231 Fourier method makes the assumption that the statistical properties of the time-series do not vary
232 with time, being stationary and constant. In such a context, the oceanographic processes do not
233 respect the stationary assumption, and there are evidences of the non-stationary nature of bio-
234 optical properties (*e.g.* b_{bp} or c_p) along a single year (*Antoine et al.*, 2011; *Gernez et al.*, 2011;
235 *Dall’Olmo et al.*, 2012; *Barnes et al.*, 2014; *Kheireddine et al.*, 2014). But, the WA overcomes this
236 problem of non-stationary conditions by performing a local time-scale decomposition of the signal.
237 Thus, WA provides time-dependent spectra (*Lau and Weng* 1995; *Torrence and Campo*, 1998,
238 *Percival and Walden*, 2000; *Ampe et al.*, 2014). This approach helps to track how the different
239 scales are related to the periodic components of the signal. WA is applicable to stationary or non-
240 stationary time-series and quantifies correlation between two signals (*Daubechies*, 1992; *Lau and*
241 *Weng* 1995; *Cazalles et al.*, 2008; *Garcia-Reyes et al.*, 2013). Figure 3 gives an example of
242 application of WA to a stationary synthetic signal and provides elements to interpret the results
243 obtained by this analysis as well as definition of the main WA indexes.

244 Additionally, in order to understand which are the main dominant cycles that explain the variability
245 on a three-year’s time-series, the coefficient AWP* is computed as follows:

246

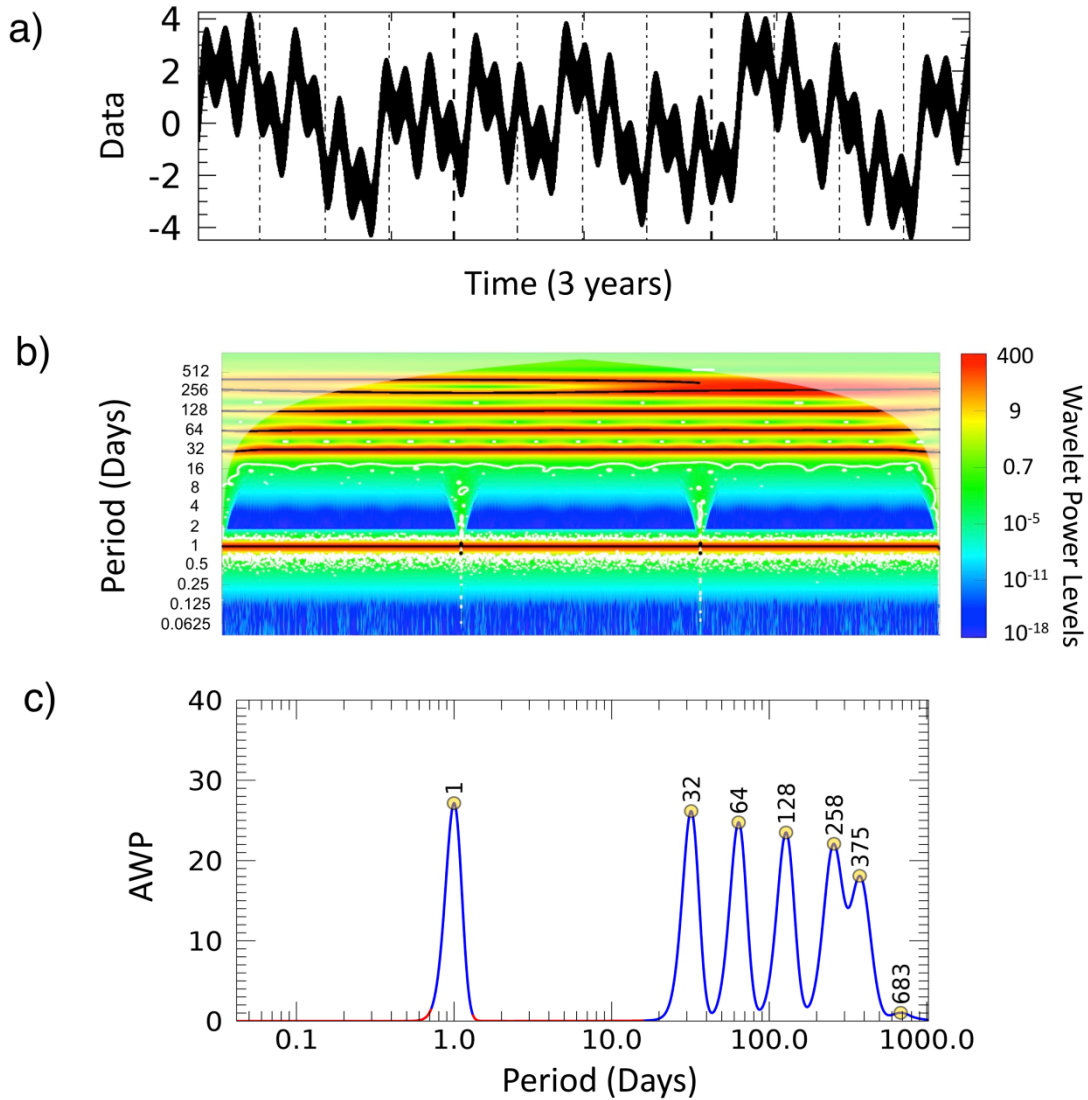
247

$$AWP_k^* = \frac{AWP_{period}}{AWP_{maximum}}$$

248

249 AWP_k^* is, thus, the ratio between the average wavelet power (AWP_{period} ; Table 1) of each local
250 maximum with respect to the absolute AWP maximum for each parameter k ($AWP_{maximum}$; Table
251 1). The ratios allow the rank of cycles for each parameter evaluating which cycles are the most
252 important (values approximately 1) and which are not (values close to 0).

253 A cross-wavelet analysis (CWA) has also been applied to paired bio-optical coefficients time-series
254 at BOUSSOLE site, which allows identification of the temporal relationship between the cycles of
255 the bio-optical properties. The CWA is fundamentally a comparison between the spectra of two
256 time-series, $x(t)$ and $y(t)$ (*Chatfield*, 1989), sampled with the same time step. It results in a quantity,
257 the cross-wavelet coherence, which can assume values between 0 and 1, indicating the cross-
258 correlation between the spectra of two time-series, as a function of the period. The most important
259 information obtained by CWA is the identification of the portions of $x(t)$ that covaries with $y(t)$ at
260 specific periods. An output from CWA, coupled to the wavelet coherence spectra (WCS), is its
261 time-average (the average coherence; AC). The AC is equal to 1 when there is a perfect linear
262 relationship at particular periods between the two time-series spectra. In this work, the CWA has
263 been used to investigate the strength of the relationship between bio-optical properties at different
264 temporal scales (*e.g.* Figs. 6, 9, 10, 11) and to understand the relative phases between the time-
265 series. For more information about the theoretical background and applications of WA and CWA
266 see *Torrence and Combo*, (1998) and *Cazalles et al.*, (2008).



267
 268 Figure 3: Theoretical example of a three-year time-series of data at 15 minutes' interval, built by overlapping
 269 6 continuous sinusoids at 1, 32, 64, 128, 256 and a two-year 365 days' cycles (a). The wavelet power
 270 spectrum (WPS) resulting from the WA is shown in (b) as a function of time. The y axis is the period and
 271 colors indicate the power levels of the time-series (high levels in red and low levels in blue). The time-series
 272 has a strong (cyclical) signal for the periods and duration of time in correspondence of the black lines in the
 273 WPS. The shaded area has not to be considered as it might provide false periodic events (*Torrence and*
 274 *Compo, 1998*). The thin white contours surrounding regions of stronger variance in the spectra indicate
 275 coherent time-frequency regions that are significant (*i.e.* > 95% significance). Panel c shows the average of
 276 WPS which is the average of the power levels for each period over the whole time-series. Local maxima in
 277 the AWP (yellow dots) indicate periods contributing significantly to the variance of the time-series,
 278 providing an efficient method to detect and identify periodicities, if present. In red are highlighted periods,
 279 and correspondent AWP, with low statistical significance (less than 95%; *Roesch and Schmidbauer, 2014*).

280
 281
 282
 283
 284
 285
 286
 287

<i>Acronym</i>	<i>Definition</i>
Chl	Chlorophyll Concentration (mg m^{-3})
$b_{\text{bp}}(\lambda)$	Particulate backscattering coefficient (m^{-1})
$c_{\text{p}}(\lambda)$	Beam attenuation coefficient (m^{-1})
Chl-Fluo	Chlorophyll-Fluorescence (RFU)
M-SSA	Multi-Channel Singular Spectral Analysis
W	Window Length (N° of observations)
M	Components
WA	Wavelet Analysis
CWA	Cross-Wavelet Analysis
WPS	Wavelet Power Spectra
AWP	Average Wavelet Power
AWP*	Average Wavelet Power Ratio
WCS	Wavelet Coherence Spectra
AC	Average Coherence

Table 1: Symbol and acronym definitions.

288

289

290 3. Results

291 This section starts from the description of each time-series, throughout the detection of the intra-
 292 annual dominant temporal patterns, and ends with the description of the changes of the main cycles
 293 over time and the definition of the temporal relationships between the different cycles of the bio-
 294 optical properties here studied.

295 3.1 Description of the time-series

296 The time-series of each parameter whose gaps are filled by using the M-SSA technique are shown
 297 in Figure 2. The b_{bp} and c_{p} range of variation is respectively between 10^{-4} m^{-1} and 10^{-3} m^{-1} and
 298 between 0.1 m^{-1} and 1.0 m^{-1} with minima occurring in the summer/fall (*i.e.* oligotrophic season) and
 299 maxima occurring in the winter/spring (*i.e.* mesotrophic season), respectively (Figure 2). The Chl-
 300 Fluo annual signal ranges between 0.012 RFU, in summer/fall, up to 7.5 RFU in winter/spring.

301 3.2 Dominant temporal patterns

302 Figure 4 and Table 2 display the AWP after the wavelet analysis on the three time-series, and the
 303 correspondent AWP*. For the Chl-Fluo nine relative maxima (yellow circles in Figure 4a) emerge
 304 at periods of approximately 351, 200, 124, 46, 31, 21, 10, 3 and 1 days, indicating nine major
 305 patterns of the Chl-Fluo variability. The AWP spectrum for b_{bp} shows seven relative maxima at
 306 370, 193, 126, 58, 16, 11, 2 days. Finally, for the c_{p} relative maxima at 372, 192, 130, 57, 27, 15,
 307 11, 4, 2, 1 days are detected. In both cases of b_{bp} and c_{p} , two additional maxima are found at 979
 308 and 911 days, respectively. These relative maxima have low AWP (<1) and are related to periods
 309 exceeding the upper limit that can be significantly retrieved in this study (*i.e.* 1 year).

310 For brevity, periods close to 365 days are interchanged with the term “annual”, close to 180-days
 311 with “6-months”, close to 128-days with “4-months”.

312 3.3 Wavelet Power Spectra

313 The WPS of Chl-Fluo (Figure 5a) reveals a persistent annual periodicity, thereby explaining the
 314 greatest amount of variability. Accordingly, the AWP value shows its maximum (30.8) at this

315 period (Table 2) with two secondary maxima at 4-months and at 6-months, both accounting for half
316 of the variability with respect to the annual periodicity (14.6 and 15.6 respectively; Table 2).

317 In the case of b_{bp} , the annual cycle has an AWP value of 24.3. The most dominant patterns are
318 associated to the 6-month cycle with an AWP of 29.7, and 4-month cycle with AWP of 24.3 (Figure
319 4). A significant cycle is also present with a period of 58 days (AWP value of 11.0). The WPS
320 (Figure 5b) highlights a range between 11 and 16 days, particularly evident at the winter-to-spring
321 transitions, with a clear inter-annual variability and the AWP value for this cycle is less than 5
322 (Figure 4). For cycles between 0.5 and 2 days, the AWP is generally lower, yet not zero, indicating
323 that some periodicity for b_{bp} at these scales exists though with limited impact on the overall
324 variability (Table 2). Cycles less than 2 days also have less statistical significance along the three
325 years of data.

326 The c_p cycles at 4-months, 6-months, and 1-year periods are observed in the WPS (Figure 5c),
327 resulting in AWP values of 20.3, 33.0 and 31.8, respectively (Figure 4 and Table 2). Other relative
328 maxima have average values less than 6. The WPS (Figure 5c) also highlights 1, 2, 4, 11-15, 27 and
329 57 day cycles, evident at the transition from winter to spring of 2012. For the period at 1 day, the
330 AWP is low, though greater than zero, and still statistically significant, indicating that some c_p
331 variability at this scale exists (Table 2).

332 The signal of the annual cycle covers all seasons for all parameters (Figure 5), which have maxima
333 at a particular moment of the year: always in winter and spring (Figure 2 and Figure 5). The 6-
334 month period is the dominant pattern in the case of b_{bp} and c_p , and is the second dominant pattern in
335 the Chl-Fluo time-series. The 4-month cycle shows a considerable magnitude for b_{bp} and c_p , but is
336 limited for Chl-Fluo (Table 2). Moving to the lowest temporal cycles, Figure 5 shows how diel
337 cycles are detectable for most of the three time-series, confirming the importance of this temporal
338 scale, especially for Chl-Fluo and c_p time-series.

339 Summarizing, Chl-Fluo shows a strong annual cycle signal along the entire time-series, but
340 particularly from spring 2011 to winter 2013 considering only the lightened areas (Figure 5a). The
341 year 2012 (more specifically from winter 2011 to spring 2013) shows a strong cyclic nature at
342 periods greater than 1 week.

343 WPS of b_{bp} shows high power levels from 128 to 365 day periods (Figure 5b). However, for periods
344 lower than 64-days, the strength of the WPS is high only during spring and winter.

345 Contrarily, WPS of c_p (Figure 5c), shows evident inter-annual variability yet not all the temporal
346 footprints (*i.e.* periods) have high values in 2011 and 2013. Dominant cycles are persistent at higher
347 temporal scales from 2011 to 2013, whereas periods lower than 64 days are dominant only in the
348 winter and spring in agreement with the other bio-optical properties.

349 The Chl-Fluo AWP is also characterized by two relative maxima in correspondence with 46 and
350 124 days (Table 2), occurring only in the mesotrophic periods of the year (winter – spring of 2012;
351 Figure 5a). The AWP of b_{bp} shows relevant cycles also at the 11-16, 58 and 126 day periods
352 occurring in the most productive periods of the year of 2011 – 2013 (winter and spring).
353 Furthermore, the 126-day cycle has a strong influence on the entire time-average spectrum (Figure
354 4 and 5b). In case of c_p , there is a relevant cycle at 130 days. All these cycles have strong signals
355 during the winter and spring seasons (Figure 5). In such a context, Figure 6 illustrates the AC
356 obtained with the CWA between the different bio-optical coefficients along the entire 3-year time-
357 series of observations. A high correlation (> 0.8) between the periodicities of bio-optical
358 coefficients greater than 10 days is observed (Figure 6). Periodicity at these scales has been poorly
359 represented in the literature, and with the use of WA all of these cycles can be retrieved and

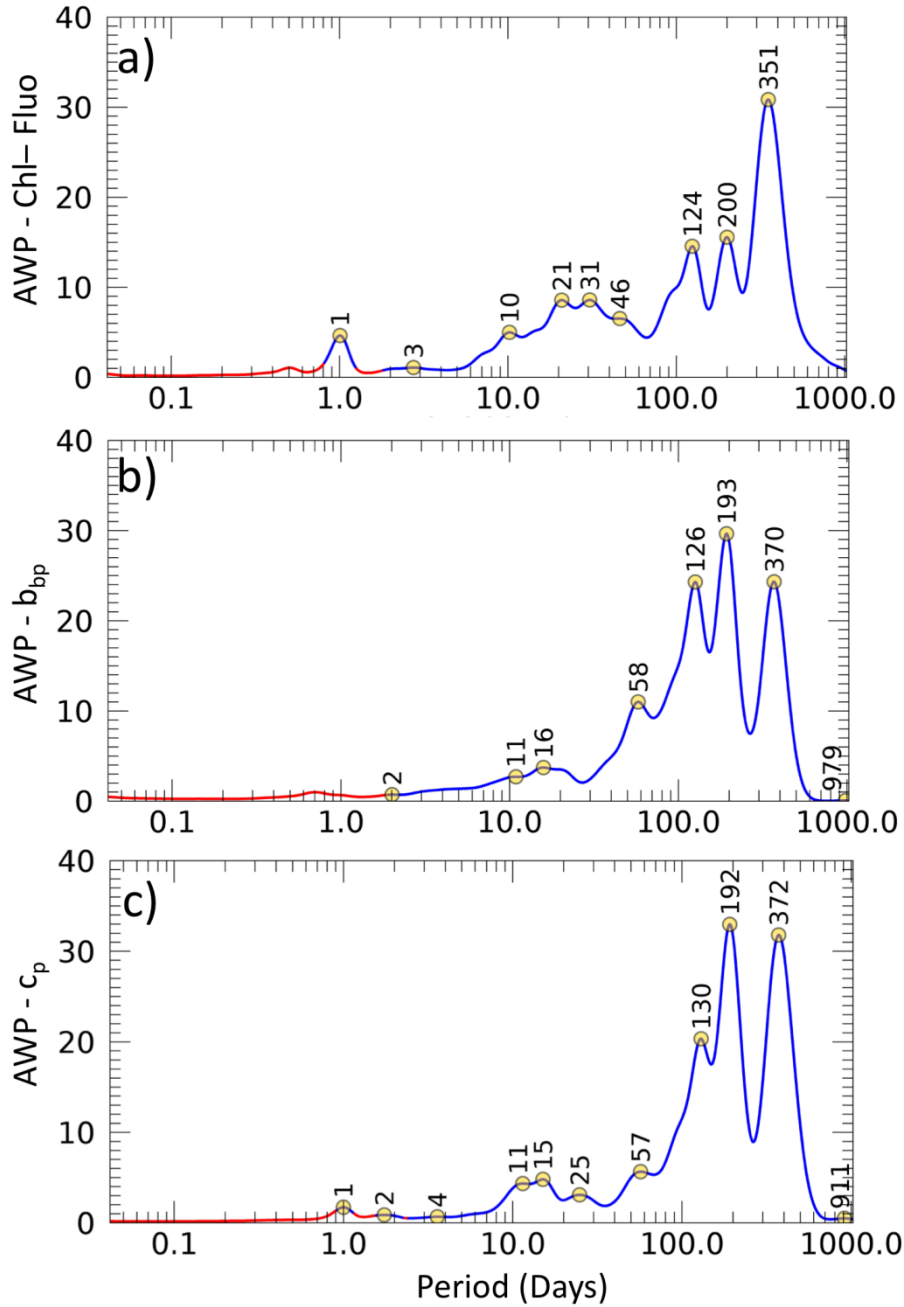
360 described. Figure 5 displays evident cycles in winter 2012 for all parameters (black lines; *i.e.* a
361 productive period), and, therefore, it is an optimum case of study to highlight those lesser-known
362 cycles, such as the intra-seasonal cycles (*i.e.* diel, weekly, monthly). In order to complement the
363 analysis, an opposite case of study has been analyzed by applying a specific WA on summer 2012,
364 *i.e.* the most oligotrophic period. Moreover, in these seasons, the diurnal variance of parameters is,
365 in general, the highest in winter and the lowest in summer (*not shown*). Finally, the selected data
366 sets have a limited number of missing observations (less than 11 % in both winter and summer
367 seasons), restricting the use of reconstructed measurements.

368 In order to highlight the mid and short-term variability, a specific WA has thus been applied to two
369 selected seasons of the time-series: winter and summer 2012 (Figures 7 and 8). Figure 7 shows the
370 AWP obtained by WA on winter 2012 and Table 3 contains the AWP* values correspondent to the
371 maxima. For the b_{bp} , four significant maxima are retrieved (yellow circles in Figure 7a) at periods of
372 17, 10, 5 and 1 days indicating four major patterns of b_{bp} variability in this season. There is also a
373 12 hour cycle that emerges from the analysis, but with reduced statistical significance in respect to
374 other cycles (less than 95%). The c_p AWP shows five relative maxima at 29, 12, 3, 2, and 1 days. A
375 diel cycle is evident and represents the third maximum even if with a low AWP. Ultimately, for the
376 Chl-Fluo, detected relative maxima are 29, 18, 11, 3 and 1 days. In winter, the dominant temporal
377 patterns are of cycles greater than 10 days for all three parameters.

378 The opposite season, summer, is the counterpart case of study. This is the period of lowest
379 productivity along the entire year at BOUSSOLE site. Figure 8 shows a time-series for each
380 parameter and the corresponding AWP and AWP* (Table 4). For the b_{bp} different maxima emerged
381 (yellow circles in Figure 7a) in correspondence to 18, 10, 7, 4, 2, 1 days and 12 hours indicating
382 these cycles as the main driven temporal patterns of variability during the season. The diel cycle is
383 the second important temporal pattern for this coefficient. The c_p AWP shows five relative maxima
384 at 23, 10, 4, 3, 1 days. The diel cycle is the most dominant for c_p in summer (AWP of 22.0). Lastly,
385 the Chl-Fluo has eight relative maxima at 22, 12, 8, 4, 3, 1 days and 12 hours and the diel cycle is
386 the most significant local pattern. One could argue that, during summer, the quenching effect can
387 dominate and drive the diel cycle of Chl-Fluo. Therefore, this has to be taken into account in the
388 interpretation of the results for the Chl-Fluo diel cycle (*Xing et al., 2017*).

389 **3.4 Cross-Wavelet Analysis**

390 The Chl-Fluo vs b_{bp} time-series have high AC values for periods ranging from 1 day ($\cong 0.7$) to 1
391 year ($\cong 1$). At lower scales, there is a high correlation only during the winter and spring (Figure 9).
392 This is also true for the Chl-Fluo vs c_p and the c_p vs b_{bp} time-series which have coherence values 0.7
393 and 0.8 for the 1 day period, respectively, and up to $\cong 1$ at the annual scale. At periods lower than 1
394 day, the correlation between the three bio-optical parameters is low (<0.5). The Chl-Fluo to c_p
395 coherence analysis reveals that the correlation is higher at daily scales (> 0.7) with respect to Chl-
396 Fluo/ b_{bp} . The AC value is higher with respect to Chl-Fluo and b_{bp} . This is confirmed by what is
397 expected about the relationship between b_{bp} and phytoplankton cells (*Loisel et al., 2001; Stramski et*
398 *al., 2004, Dall'Olmo et al., 2009; 2012*).

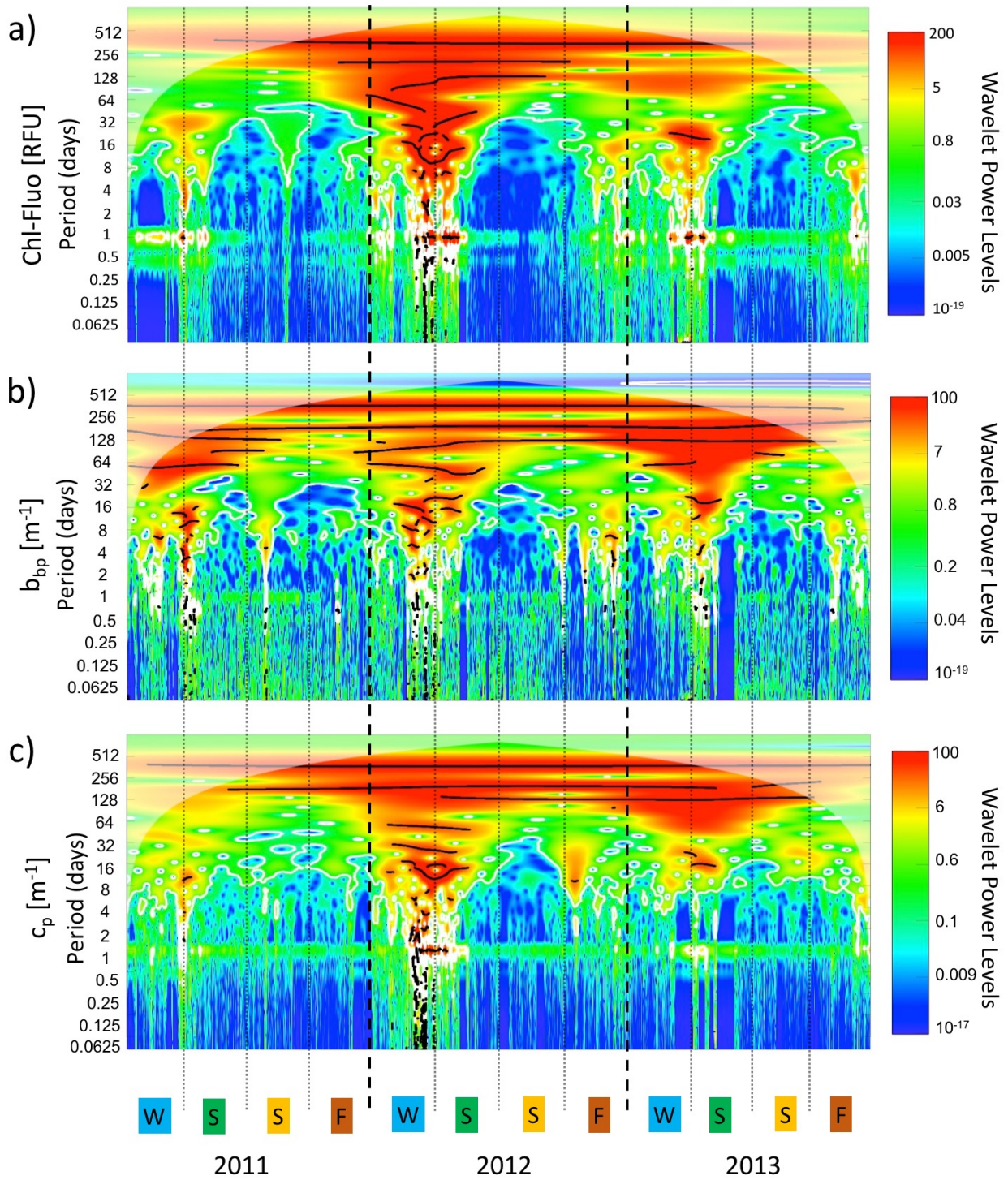


399

400 Figure 4: AWP of the Chl-Fluo (a), b_{bp} (b) and c_p (c). The statistical significance is 95% in case of the
 401 highest temporal scales, from day to annual scales, for each parameter (blue line). At the lowest temporal
 402 scales, the significance is lower than 95% (red line) and the results have to be interpreted with caution. The
 403 statistical significance is computed following *Roesch and Schmidbauer* (2014). Yellow dots are the relative
 404 local maxima for the single parameter with also information of the exactly days.

Period (days)	351	200	124	-	46	31	21	-	10	3	-	1
$AWP_{Chl-Fluo}^*$	1.0	0.50	0.47	-	0.21	0.27	0.27	-	0.16	0.05	-	0.15
Period (days)	370	193	126	58	-	-	-	16	11	-	2	-
$AWP_{b_{bp}}^*$	0.82	1.0	0.82	0.37	-	-	-	0.13	0.09	-	0.02	-
Period (days)	372	192	130	57	-	-	25	15	11	4	2	1
$AWP_{c_p}^*$	0.96	1.0	0.62	0.17	-	-	0.09	0.15	0.13	0.02	0.03	0.05

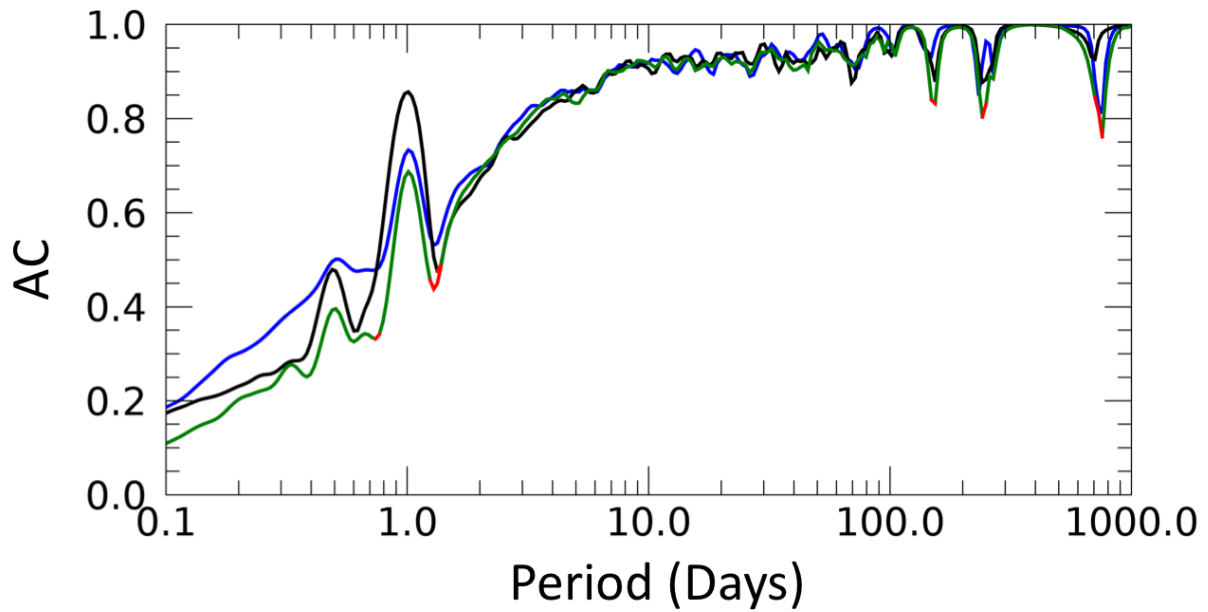
405 Table 2: AWP* from the AWP of each parameter. Numbers in bold indicate the dominant cycles.



407

408 Figure 5: WPS for Chl-Fluo (a), b_{bp} (b) and c_p (c). The letters W stands for winter (in blue), S for spring (in
 409 green), S for summer (in orange) and F for fall (in brown). The time-series has a strong (cyclical) signal for
 410 the periods and duration of time in correspondence of the black lines in the WPS. The shaded area has not to
 411 be considered as it might provide false periodic events (*Torrence and Compo, 1998*). The thin white contours
 412 surrounding regions of stronger variance in the spectra indicate coherent time-frequency regions that are
 413 significant (*i.e.* 95% significance). The significance test is computed following *Roesch and Schmidbauer*
 414 (*2014*).

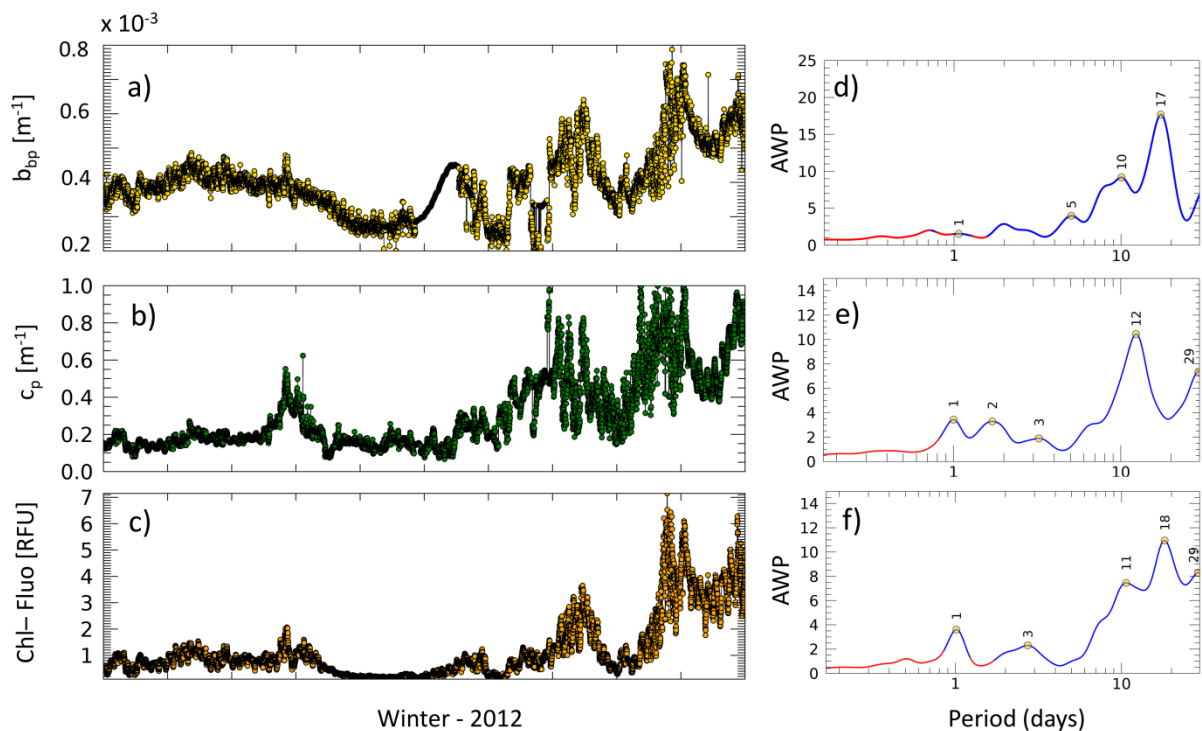
415



416

417 Figure 6: AC obtained from the CWA between paired bio-optical properties: Chl-Fluo vs. b_{bp} (green line),
 418 Chl-Fluo vs. c_p (black line) and b_{bp} vs. c_p (blue line). In red are highlighted periods where the AC is with low
 419 statistical significance (less than 95%).

420



421

422 Figure 7: Time-series of b_{bp} (a), c_p (b) and Chl-Fluo (c) in Winter 2012. AWP of b_{bp} , c_p , Chl-Fluo are in
 423 panels d, e, f. Red lines are located where the statistical significance is less than 95% and the results have to
 424 be interpreted with caution. The significance test is computed following *Roesch and Schmidbauer (2014)*.

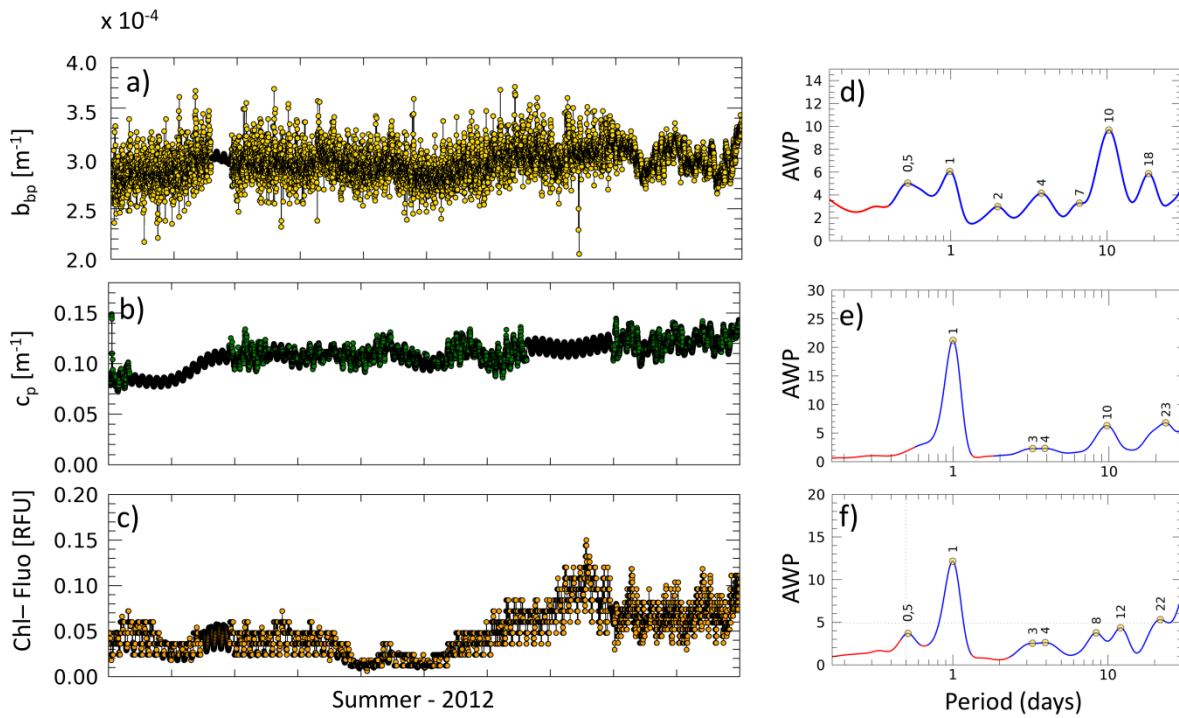
425

426

Period (days)	-	17	10	5	-	1
$AWP_{b_{bp}}^*$	-	1.0	0.52	0.23	-	0.09
Period (days)	29	-	12	3	2	1
$AWP_{c_p}^*$	0.70	-	1.0	0.18	0.31	0.33
Period (days)	29	18	11	3	-	1
$AWP_{Chl-Fluo}^*$	0.76	1.0	0.68	0.21	-	0.33

427 Table 3 AWP* from the AWP of each parameter in Winter 2012. Numbers in bold indicate the dominant
428 cycles.

429



430 Figure 8: Time-series of b_{bp} (a), c_p (b) and Chl-Fluo (c) in Summer 2012. AWP of b_{bp} , c_p , Chl-Fluo are
431 reported in panels d, e, f. Red lines are located where the statistical significance is less than 95% and the
432 results have to be interpreted with caution. The significance test is computed following *Roesch and*
433 *Schmidbauer* (2014).
434
435

Period (days)	18	10	7	4	2	1	0.5
$AWP_{b_{bp}}^*$	0.61	1.0	0.34	0.43	0.31	0.63	0.52
Period (days)	23	10	-	4	3	1	-
$AWP_{c_p}^*$	0.32	0.30	-	0.11	0.11	1.0	-
Period (days)	22	12	8	4	3	1	0.5
$AWP_{Chl-Fluo}^*$	0.44	0.36	0.31	0.22	0.21	1.0	0.30

436 Table 4: AWP* from the AWP of each parameter for Summer 2012. Numbers in bold indicate the dominant
437 cycles.

438

439

440 4. Discussion

441 4.1 Annual cycle

442 The most generally observed pattern was a phytoplankton maximum in the winter/spring season,
443 minimum in summer and a successive increase in fall season, that corresponds to a typical annual
444 cycle of a temperate ocean, as already reported for the north-western Mediterranean Sea (*Antoine et*
445 *al.*, 2011; *D'Ortenzio et al.*, 2014).

446 The main pattern revealed by WA applied to BOUSSOLE data is the periodicity of the seasonal
447 evolution: from late fall to early spring (essentially the winter) where there is always a convergence
448 of Chl-Fluo, b_{bp} and c_p signals (Figures 5 and 9).

449 The spring bloom in the Ligurian Sea is regulated by the increase of light availability after the
450 winter mixing of the water column that redistributes nutrients from deep to surface waters (*Antoine*
451 *et al.*, 2011; *D'Ortenzio et al.*, 2014). The phasing, duration and intensity of the annual bloom
452 varies from year to year, with a stronger bloom in 2012 in respect to 2011 and 2013 (Figure 2;
453 *Mayot et al.*, 2016). This variability arises from the range of the processes controlling bloom
454 dynamics, including physical forcing such as meteorological extreme events, and/or interaction
455 between different species of phytoplankton organisms (*Winder et al.*, 2010).

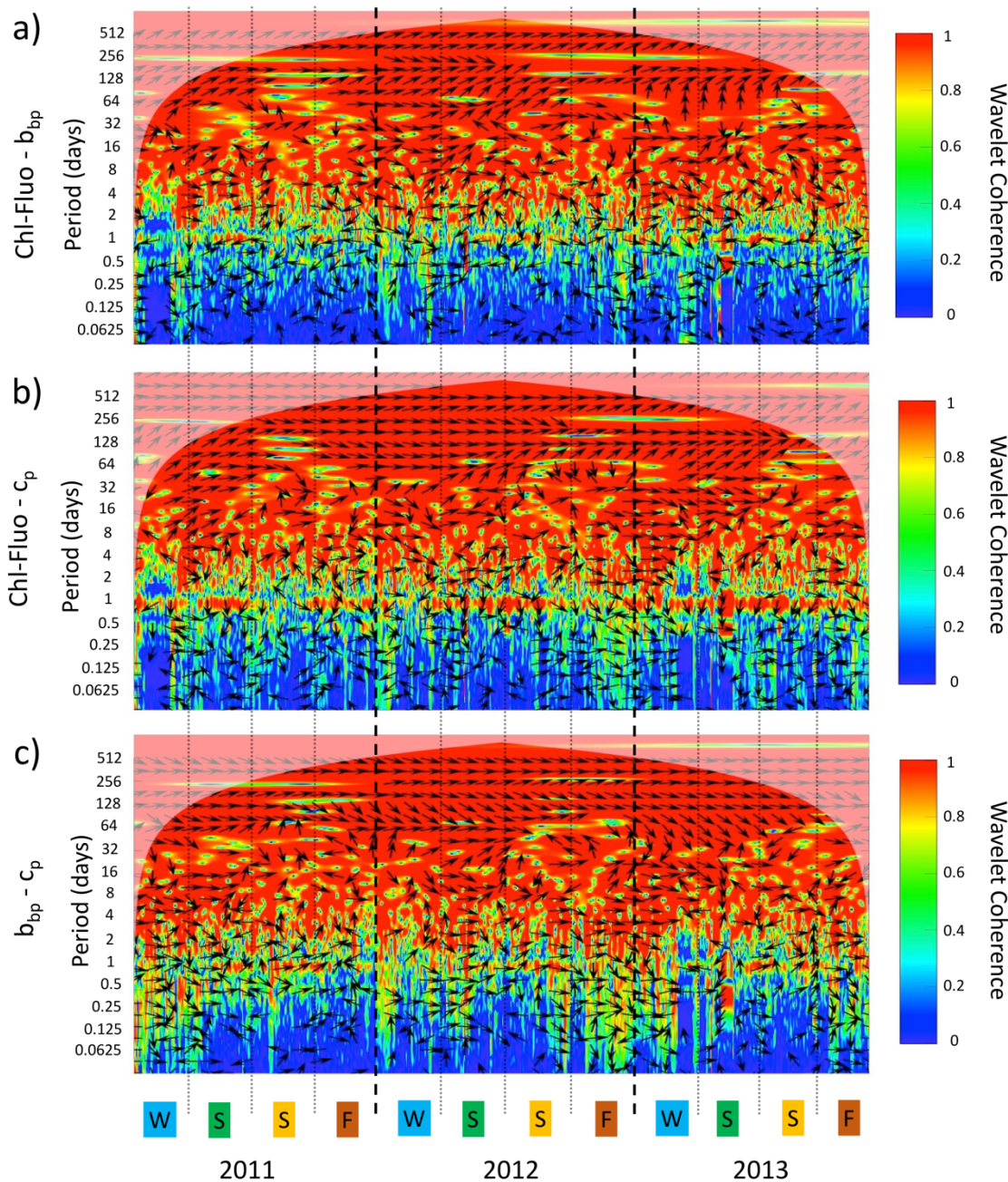
456 During summer, the increase of light availability causes the decrease of intra-cellular photosynthetic
457 pigments concentration need and, concurrently, the low nutrient availability limits the
458 phytoplankton population growth and its abundance stays low (*Bellacicco et al.*, 2016). The b_{bp} and
459 c_p are characterized by a similar temporal pattern in summer (Figure 2 and 5). During fall, as light
460 availability decreases and mixed layer deepens, phytoplankton concentration increases again.

461 The b_{bp} and c_p time-series are coherent with the Chl-Fluo time-series at annual scale because both
462 b_{bp} and c_p are sensitive to particle size ranges that include phytoplankton (*Stramski et al.*, 2004;
463 *Sosik et al.*, 2008; *Organelli et al.*, 2018), thus phytoplankton cells abundance strongly impacts the
464 variability of b_{bp} and c_p . Figures 6 and 9 reveal how the bio-optical properties have a WCS and AC
465 close to 1 at annual scale along the entire time-series. In detail, Chl-Fluo is in advance in respect to
466 the annual signal of b_{bp} (Figure 9a), while with c_p they are in phase (Figure 9b). The c_p leads in
467 respect to the b_{bp} annual signal as highlighted by the arrows in the Figure 9c. In such a context, the
468 maximum of Chl-Fluo is in shift in advance of approximately 20 days with respect to c_p and b_{bp}
469 (Figure 4 and Table 2). This could be attributed to the inter-annual variability (low bloom maxima
470 in 2011 and two maxima in 2013 for Chl-Fluo) which determined a dephasing in the AWP. Another
471 reasonable explanation can be that the Chl-Fluo annual maximum (independently of its strength) is
472 not occurring always at the same time (*i.e.* indeed there are four maxima in the Chl-Fluo time-
473 series: March in 2011 and 2012, April and December in 2013; Figure 2). Nevertheless, there is a
474 good coherence between the parameters at annual temporal scales ($AC \cong 1$; Figure 6).

475 4.2 Six- and four- month cycles

476 Other fundamental cycles retrieved by WA are at 6 months and 4 months. The 6-month cycle is
477 unexpectedly the most important cycle in cases of b_{bp} and c_p , while for Chl-Fluo it is second in
478 terms of dominance. The 4-month cycle is the third important cycle for all of the parameters,
479 especially for b_{bp} (Table 2). AC shows a strong correlation of the WPS for all combinations of bio-
480 optical coefficients at these periods ($\cong 1$; Figures 6 and 9). The 6-month cycle is dominant for b_{bp}
481 and c_p , whereas it has a lower strength for the Chl-Fluo, a consequence of the inter-annual
482 variability of its WPS (Figure 5a). The 6- and 4-month cycles are interpreted here as mainly due to

483 the winter-to-spring modification of the mixing intensity (*D'Ortenzio et al., 2005*), nutrient and
484 light availability, grazing and shift in phytoplankton community structures (*Mignot et al., 2014;*
485 *Sammartino et al., 2015*). *Bellacicco et al., (2016)* highlight that the use of Chl as a proxy of
486 phytoplankton biomass, as well as Chl-Fluo, is strictly influenced by intracellular processes,
487 especially in intermediate seasons, such as late spring and early fall. Alternately, b_{bp} and c_p are
488 sensitive to the abundance of phytoplankton cells and non-algal particles, as well as particle size
489 distribution, refractive index, and the shape and structure of particles in the seawater. Therefore, in
490 these intermediate periods, where the Chl-Fluo signal is low while c_p and b_{bp} are relatively high, the
491 6-month cycle signal detection could be reduced impacting total seasonal and annual cycles. For
492 example, in early fall, there are low nutrients and low light conditions and the result is an increase
493 of phytoplankton cells, as indicated by the increase of c_p and b_{bp} , however phytoplankton does not
494 have a high concentration of photosynthetic pigment, and consequently a low Chl-Fluo. In late
495 spring, the photoacclimation process is particularly relevant and impacts on Chl-Fluo due to high
496 nutrients and high light availability. The b_{bp} and c_p proxies are not affected by the phytoplankton
497 physiological state (*Bellacicco et al., 2016; Barbieux et al., 2018*) and the effect of the carbon
498 accumulation in phytoplankton cells dominates the c_p and b_{bp} WPS (Figures 4 and 5b, c), while the
499 physiological signal (*i.e.* photoacclimation) has an effect on the strength of the signal in WPS of the
500 Chl-Fluo signal (Figures 4 and 5a). Figure 9 displays how c_p signal is in advance with respect to b_{bp}
501 at 6 month cycles along 2012 and 2013. On the other hand, the b_{bp} signal is in delay in respect to
502 Chl-Fluo in 2012, while with c_p they are in phase from summer 2011 to spring 2012. Figure 9 also
503 shows the relationship between parameters at the period of 4-months. In this period, Chl-Fluo signal
504 is delayed in respect to c_p as in the case of 6-months, while c_p signal seems to be in advance
505 compared to the b_{bp} signal. From the analysis, the intensity of a 4-month cycle differs in cases of
506 Chl-Fluo in respect to b_{bp} and c_p (Table 2).



507
 508 Figure 9: Cross-wavelet coherence spectra between (a) Chl-Fluo and b_{bp} , (b) Chl-Fluo and c_p , and (c) b_{bp} and
 509 c_p at BOUSSOLE site. Color indicates the level of covariability between the time-series (values between 0
 510 and 1); arrows denote the relative phase between the time-series (right: in phase; left: antiphase; up or down:
 511 one series leads the other by 90°) with significance covariability ($> 95\%$). Shaded area has not to be
 512 considered as it might provide false periodic events (*Torrence and Compo, 1998*). The letters W stands for
 513 winter (in blue), S for spring (in green), S for summer (in orange) and F for fall (in brown), as for Figure 5.

514
 515 **4.3 Intra-seasonal variability: mid- and short-term cycles**

516 WA detected relevant cycles at scales other than annual, 6- and 4-months are interpreted here as
 517 caused by intra-seasonal (*i.e.* from diel to monthly) variability of the examined bio-optical
 518 parameters: the highest cycles are defined as mid-term cycles, while the lowest as short-term
 519 counterparts. In such a context, the specific WA applied to these particular periods of winter and

520 summer 2012 enables the detection and power of these additional sources of variability (from 12
521 hours to 29 days; Tables 3 and 4).

522 At the beginning of winter and over the 16 day period, c_p and Chl-Fluo signals are in phase and then
523 c_p is in advance compared to the Chl-Fluo footprint. Contrarily, b_{bp} and Chl-Fluo indicators are in
524 phase along the entire season. From 2 day up to 16 day periods, Chl-Fluo is partially in phase with
525 b_{bp} and c_p , however, some hotspots occur in which both b_{bp} and c_p have phase differences in respect
526 to the Chl-Fluo signal. In cases of b_{bp} to c_p , at these highest periods, c_p leads the b_{bp} mark (Figure
527 10).

528 In summer, at the range of 8-16 days, Chl-Fluo is in advance in respect to the b_{bp} signal, while on
529 the reverse, the Chl-Fluo indicator at this period is delayed with respect to the c_p . Regarding the b_{bp}
530 to c_p relationship, the former is in advance with respect to the latter at the beginning of summer,
531 while at the end of summer, there is an opposite situation of delay. Between 2 and 8 days, Chl-Fluo
532 is not in phase with both c_p and b_{bp} signals (*e.g.* start of summer), while the optical parameters are in
533 phase (Figure 11).

534 A possible explanation of these mid-term cycles could also be given by episodic phytoplankton
535 biomass increases in response to stochastic events that potentially impact the mixed layer dynamics
536 which are typical of the winter period at the BOUSSOLE site. For instance, as highlighted by
537 *Winder et al.*, (2010), extreme wind events could generate biomass oscillations by temporarily
538 reducing the phytoplankton bloom. In addition, *Nezlin et al.* (2002) showed, using WA, that short-
539 period variations (less than 100 days) of remotely-sensed chlorophyll during spring seasons
540 correlated with surface water, air temperatures and wind stress, that have rapidly varied (*i.e.* at the
541 intermediate scales that we analyze here). The mechanism of these variations was an intensification
542 of phytoplankton growth resulting from mixing of the water column by wind stress and entrainment
543 of cold, rich in nutrients, water into the euphotic layer. *Monteiro et al.* (2015) demonstrated the
544 presence of an intra-seasonal variability that is always driven by wind stress and has a temporal
545 scale from daily up to 14 - 20 days. These orders of magnitude are consistent with the maxima
546 reported in the AWP plots, for both winter and summer 2012 (Figures 7, 8; Table 3 and 4).

547 The general Chl-Fluo and c_p WPS also show a clear diel cycle footprint, particularly evident during
548 high biomass periods (winter and spring in Figure 5a and c). On the other hand, the diel signal is
549 less evident for b_{bp} (Figures 4 and 5b and Table 2). The correlation between c_p and Chl-Fluo at diel
550 scale (AC greater than 0.7 in Figure 6) is well known during winter and spring, when the particles
551 abundance is dominated by phytoplankton cells (*Kheireddine et al.* 2014; *Bellacicco et al.*, 2016).
552 The diel changes are generally considered to be driven by specific forcings (*Oubelkheir et al.*, 2005;
553 *Oubelkheir and Sciandra* 2008; *Gernez et al.*, 2011, *Loisel et al.*, 2011; *Barnes et al.*, 2014;
554 *Kheireddine et al.*, 2014). At diel cycle, the correlation between Chl-Fluo and b_{bp} periodicities is
555 lower ($\cong 0.6$) than to Chl-Fluo vs. c_p (>0.7). A good correlation is found in the b_{bp} vs c_p (>0.7).

556 By applying the specific WA over a three-month period both in winter and summer seasons, more
557 information can be gathered about short-term variability, especially on the diel cycle.

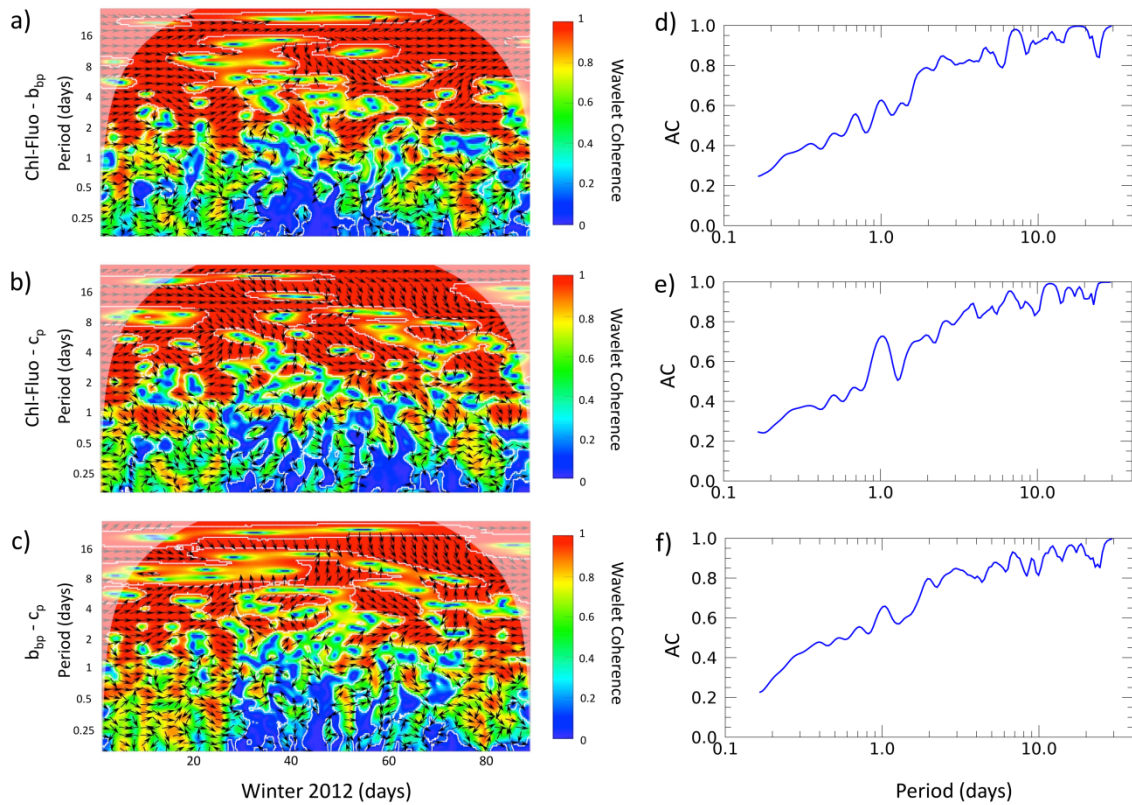
558 During the winter, Chl-Fluo signal is in advance to c_p without any phases between parameters
559 despite AC showing high values (Figure 10). Reversely, the AC between Chl-Fluo and b_{bp} is lower
560 (less than 0.5) below diel cycle. The AC between b_{bp} and c_p is always lower than 0.6 (Figure 10).

561 In the winter, the period of strong mixing and start of the bloom (*Barnes et al.*, 2014, *Kheireddine*
562 *et al.* 2014; *Bellacicco et al.*, 2016), c_p can be increasingly influenced by diel variations of
563 abundance of phytoplankton cells (*Oubelkheir et al.*, 2005, *Oubelkheir and Sciandra*, 2008), even if
564 with a marginal impact on total variability (Table 3). In contrast to c_p , b_{bp} diel cycle is not marked

565 by a significant seasonal variability. This would confirm that phytoplankton makes a lower
566 contribution to b_{bp} than to c_p , so their seasonal changes are poorly reflected in overall seasonal
567 changes. b_{bp} is influenced more by the presence of sub-micrometer particles such as detrital
568 particles or heterotrophic bacteria (*Morel and Ahn, 1991; Stramski and Kiefer, 1991, Stramski et*
569 *al., 2004*), that do not have a periodical diel cycle. Recently, *Organelli et al., (2018)* found that
570 another main source of variability on b_{bp} is due to particles with equivalent diameters between 1 and
571 10 μm giving thus new insight into the b_{bp} coefficient and particles in seawater.

572 In summer, Chl-Fluo and b_{bp} have an AC of 0.8 but b_{bp} is largely in anti-phase with Chl-Fluo, as
573 expected for this period of year of low productivity. Inversely, c_p and Chl-Fluo diurnal signals have
574 an AC value of approximately 1. During this season of absence of high abundance of phytoplankton
575 (*Kheireddine et al. 2014; Bellacicco et al., 2016*), c_p can be due to the daily variations of coupled
576 heterotrophic bacteria and particles pool (*i.e.* phytoplankton cells) which remain within the upper
577 layer caused by the strong stratification of the water column. However, Chl-Fluo diel signal can be
578 determined due to the quenching effect (*Xing et al., 2017*). In addition, at periods of 0.5 (*i.e.* 12
579 hours), c_p and b_{bp} signals are in anti-phase with Chl-Fluo. Due to this limited productivity, cycles
580 greater than 1 day are not the most impactful of the intra-seasonal variability, while conversely the
581 diurnal signal is well pronounced. *Oubelkheir and Sciandra (2008)* argued that the diel cycle of c_p ,
582 and the particles pool, is strictly influenced by changes in the properties of particles (*e.g.* size,
583 refractive index, shape and internal structure) and also by external environmental and biological
584 agents, as reported by *Binder and Durand (2002)*. During daytime, phytoplankton cells fix external
585 inorganic carbon into organic molecules determining an increase of their diameter and refractive
586 index (*Siegel et al., 1989; Stramski and Reynolds, 1993; Walsh et al., 1995*), and as a consequence
587 an increase of scattering and attenuation cross section. This was also confirmed by laboratory
588 experiments on a few phytoplankton species (*Stramski et al., 1995; Durand and Olson, 1998;*
589 *Claustre et al. 2002; Poulin et al., 2018*). During night-time, phytoplankton cells divide into
590 smaller cells with lower intra-cellular carbon content, as a result of an uptake of water during
591 division or of a loss due to respiration (*Durand and Olson, 1998*). Another element to consider on
592 the c_p diel variation is the relative dynamics of algal and non-algal stocks (*i.e.* heterotrophs, viruses
593 and detritus) that could vary in relation to the season and trophic regimes. *Oubelkheir and Sciandra*
594 *(2008)* showed that the c_p is strictly related to heterotrophic particles abundance coupled with
595 phytoplankton cells and associated detritus.

596 To summarize, through the specific three-month WA, more information about detection and power
597 of these additional sources of variability can be obtained. The mid-term cycles (> 10 days)
598 dominate intra-seasonal variability during the winter (period of mixing and bloom), while they are
599 of limited impact in the case of summer which is the period of low biological production and
600 absence of extreme meteorological events (*Gernez et al., 2011, Kheireddine et al., 2014*) indicating
601 where the diel cycle is the most recurrent and important source of signal.



602

603

604

605

606

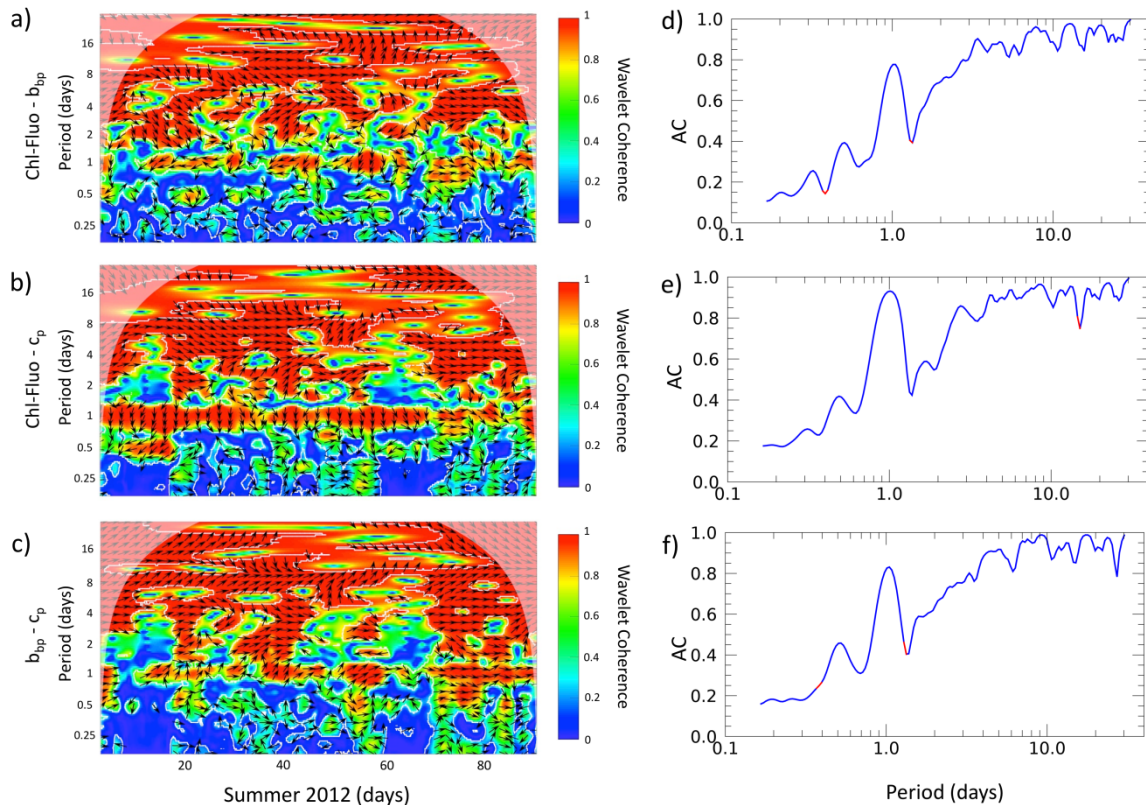
607

608

609

610

Figure 10: Cross-wavelet coherence spectra between Chl-Fluo and b_{bp} (a), Chl-Fluo and c_p (b), and b_{bp} and c_p (c) at BOUSSOLE site for the Winter 2012. Color indicates the level of covariability between the time-series (values between 0 and 1); arrows denote the relative phase between the time-series (right: in phase; left: antiphase; up or down: one series leads the other by 90°) and significance covariability ($> 95\%$ and thin white contours). Shaded area has not to be considered as it might provide false periodic events (Torrence and Compo, 1998). AC of each parameter are in Panel d-f. In red are highlighted periods where the AC is with low statistical significance (less than 95%). The significance test is computed following Roesch and Schmidbauer (2014).



611
 612 Figure 11: Cross-wavelet coherence spectra between Chl-Fluo and b_{bp} (a), Chl-Fluo and c_p (b), and b_{bp} and c_p
 613 (c) at BOUSSOLE site for the Summer 2012. Color indicates the level of covariability between the time-
 614 series (values between 0 and 1); arrows denote the relative phase between the time-series (right: in phase;
 615 left: antiphase; up or down: one series leads the other by 90°) and significance covariability ($> 95\%$ and the
 616 thin white contours). Shaded area has not to be considered as it might provide false periodic events
 617 (*Torrence and Compo, 1998*). AC for each parameter are in Panel d-f. In red are highlighted periods where
 618 the AC is with low statistical significance (less than 95%). The significance test is computed following
 619 *Roesch and Schmidbauer (2014)*.

620 5. Conclusions

621 In the last decades, the development of fixed observation sites, such as the BOUSSOLE buoy, as
 622 well as remote sensing advancement has helped to study the phenology of phytoplankton and
 623 optical properties. Several works have studied temporal variability of bio-optical properties in
 624 various oceanic regimes using both field and satellite data (*Behrenfeld et al., 2009, Antoine et al.,*
 625 *2011; Gernez et al., 2011; Barnes et al., 2014; Kheireddine et al., 2014; Behrenfeld et al. 2015;*
 626 *Sammartino et al., 2015; Di Cicco et al., 2017*). However, most of these phenological studies focus
 627 on the annual and seasonal cycles (*i.e.* long-term cycles), while there is limited literature on the
 628 mid- and short-term cycles, and their recurrence, which characterizes the temporal variability of
 629 bio-optical properties.

630 In this study, we have focused on bio-optical properties using, for the first time, a statistical *a priori*
 631 method, as the wavelet analysis (WA) is, on three-year high frequency observations. The main
 632 goals are to determine the intra-annual dominant temporal patterns of the bio-optical parameters,
 633 the changes of these cycles over time, the characteristics and recurring strength at those periods and
 634 to define the temporal relationship between the cycles of the bio-optical properties.

635 The WA applied here reveals a persistent annual cycle for Chl-Fluo which explains the largest
 636 amount of its variability. On the other hand, and unexpectedly, the 6-month cycle is the most

637 important and dominant temporal pattern of the b_{bp} and c_p time-series, with respect to Chl-Fluo,
638 which accounts for half of the variability in respect to the annual cycle. Together with 6-month, the
639 4-month cycle is the third source of variability for all the parameters with different strengths. It has
640 a particular recurrence and magnitude in the case of b_{bp} , with respect to Chl-Fluo and c_p and intra-
641 seasonal variability is driven by mid- and short-term cycles. During the winter (season of mixing),
642 the mid-term cycles (> 10 days) are the most important. Episodic bloom events can determine these
643 cycles, as viewed in the case of bio-optical coefficients, and as also found by *Winder et al.* (2010).
644 During summer, the diel cycle is the most important and the main source of variability, especially
645 for c_p and Chl-Fluo. Considering the entire time-series, at diel scale, the coherence between spectra
646 of bio-optical coefficients diminishes in respect to annual and seasonal cycles although remaining
647 high. Chl-Fluo - c_p and b_{bp} - c_p periodicities have a strong temporal correlation in respect to Chl-
648 Fluo- b_{bp} . At diurnal scale, Chl-Fluo depends specifically on intra-cellular and physiological
649 processes in relation to physical forcing, and on phytoplankton cells abundance. The c_p at the same
650 scale has its own temporal pattern: in summer, c_p is driven mostly by heterotrophic bacteria coupled
651 with low phytoplankton abundances, while in winter, c_p is more associated with phytoplankton
652 particles (*Oubelkheir et al.* 2005, *Oubelkheir and Sciandra*, 2008). In the case of b_{bp} , the correlation
653 between the periodicities of Chl-Fluo is lower with respect to c_p because the b_{bp} is influenced more
654 by small particles (*Stramski et al.*, 2004; *Kheireddine et al.*, 2014). In such a context, the recent
655 findings of *Organelli et al.* (2018) open challenges in understanding the complexity of marine
656 particles structure as sources of variability of the open-ocean b_{bp} signal that have to be addressed in
657 the next future in order to better constraint the use of b_{bp} observations for investigating the
658 biological carbon pump and phytoplankton phenology studies.
659 This work thus highlights the need to develop *in situ* technologies as well as new satellite sensors at
660 higher temporal resolutions (*e.g.* geostationary satellite) for biogeochemical/bio-optical
661 measurements that have been widely recognized as a priority in the optical and oceanographic
662 community. Indeed, high frequency observations could help to study, both in space and time, these
663 mid- and low-term cycles, poorly known, that currently are not taken into account in the ocean
664 color algorithms despite dominating the bio-optical variability at reduced time-series length (*i.e.*
665 within the season). Lastly, as it is demonstrated here, the importance of the use of WA as a
666 powerful instrument for studying both long or short time-series of bio-optical parameters and their
667 relationships in oceanography (*Winder et al.*, 2010, *Damarcq et al.* 2012, *Ampe et al.*, 2014,
668 *Corredor-Acosta et al.*, 2015, *Carey et al.* 2016, *Sala et al.*, 2018).

670 **Acknowledgments**

671 M. Bellacicco was supported by a postdoctoral fellowship from the *Centre Nationales d'Etudes*
672 *Spatiales* (CNES, France). Now, M. Bellacicco is at the Italian National Agency for New
673 Technologies, Energy and Sustainable Economic Development (ENEA) with a postdoctoral
674 fellowship funded by the ESA. Thanks also to European Space Agency (ESA) and CNES for
675 funding the BOUSSOLE project, and to all the OMTAB staffs for BOUSSOLE maintenance.

676 Data are available at the BOUSSOLE project website: [http://www.obs-
677 vlfr.fr/Boussole/html/project/introduction.php](http://www.obs-
677 vlfr.fr/Boussole/html/project/introduction.php)

678 Additional thanks to the Dr. J. Pitarch, Dr. S. Constantin, prof. M. Scardi and prof. A. Bellacicco
679 for suggestions on this work. The authors finally wish to thank the R Core Team ([http://www.R-
680 project.org/](http://www.R-
680 project.org/)) for open source software package.

681 **References**

- 682
- 683 1. Ampe, E. M., Hestir, E. L., Bresciani, M., Salvatore, E., Brando, V. E., Dekker, A., ... &
684 Batelaan, O. (2014). A wavelet approach for estimating chlorophyll-a from inland waters with
685 reflectance spectroscopy. *IEEE Geoscience and Remote Sensing Letters*, *11*(1), 89-93.
- 686 2. Antoine, D., et al. (2006), BOUSSOLE: A joint CNRS-INSU, ESA, CNES and NASA Ocean
687 Color Calibration And Validation Activity, NASA Technical memorandum N2006 – 214147,
688 61 pp.
- 689 3. Antoine, D., F. D’Ortenzio, S. B. Hooker, G. Becu, B. Gentili, D. Tailliez, and A. J. Scott
690 (2008a), Assessment of uncertainty in the ocean reflectance determined by three satellite ocean
691 color sensors (MERIS, SeaWiFS and MODIS-A) at an offshore site in the Mediterranean Sea
692 (BOUSSOLE project), *J. Geophys. Res.*, *113*, C07013, doi:10.1029/2007JC004472.
- 693 4. Antoine, D., P. Guevel, J. F. Deste, G. Becu, F. Louis, A. J. Scott, and P. Bardey (2008b), The
694 “BOUSSOLE” buoy—A new transparent-to-swell taut mooring dedicated to marine optics:
695 Design, tests, and performance at sea, *J. Atmos. Oceanic Technol.*, *25*, 968–989, doi:10.1175/
696 2007jtech0563.1
- 697 5. Antoine, D., Siegel, D. A., Kostadinov, T., Maritorena, S., Nelson, N. B., Gentili, B., ... &
698 Guillocheau, N. (2011). Variability in optical particle backscattering in contrasting bio-optical
699 oceanic regimes. *Limnology and Oceanography*, *56*(3), 955-973.
- 700 6. Barbieux, M., Uitz, J., Bricaud, A., Organelli, E., Poteau, A., Schmechtig, C., ... & D’Ortenzio,
701 F. (2018). Assessing the Variability in the Relationship Between the Particulate Backscattering
702 Coefficient and the Chlorophyll a Concentration From a Global Biogeochemical-Argo
703 Database. *Journal of Geophysical Research: Oceans*, *123*(2), 1229-1250.
- 704 7. Barnes, M., & Antoine, D. (2014). Proxies of community production derived from the diel
705 variability of particulate attenuation and backscattering coefficients in the northwest
706 Mediterranean Sea. *Limnol. Oceanogr.*, *59*(6), 2133-2149.
- 707 8. Behrenfeld, M. J., & Boss, E. (2003). The beam attenuation to chlorophyll ratio: an optical
708 index of phytoplankton physiology in the surface ocean?. *Deep Sea Research Part I:
709 Oceanographic Research Papers*, *50*(12), 1537-1549.
- 710 9. Behrenfeld, M. J., Boss, E., Siegel, D. A., & Shea, D. M. (2005). Carbon-based ocean
711 productivity and phytoplankton physiology from space. *Global biogeochemical cycles*, *19*(1).
- 712 10. Behrenfeld, M. J., & Boss, E. (2006). Beam attenuation and chlorophyll concentration as
713 alternative optical indices of phytoplankton biomass. *Journal of Marine Research*, *64*(3), 431-
714 451.
- 715 11. Behrenfeld, M. J., Westberry, T. K., Boss, E. S., O’Malley, R. T., Siegel, D. A., Wiggert, J. D.,
716 ... & Moore, J. K. (2009). Satellite-detected fluorescence reveals global physiology of ocean
717 phytoplankton. *Biogeosciences*, *6*(5).
- 718 12. Behrenfeld, M. J. (2010). Abandoning Sverdrup's critical depth hypothesis on phytoplankton
719 blooms. *Ecology*, *91*(4), 977-989.
- 720 13. Behrenfeld, M. J., O’Malley, R. T., Boss, E. S., Westberry, T. K., Graff, J. R., Halsey, K. H., ...
721 & Brown, M. B. (2016). Reevaluating ocean warming impacts on global phytoplankton. *Nature
722 Climate Change*, *6*(3), 323-330.
- 723 14. Bellacicco, M., Volpe, G., Colella, S., Pitarch, J., & Santoleri, R. (2016). Influence of
724 photoacclimation on the phytoplankton seasonal cycle in the Mediterranean Sea as seen by
725 satellite. *Remote Sensing of Environment*, *184*, 595-604.
- 726 15. Bellacicco, M., Volpe, G., Briggs, N., Brando, V., Pitarch, J., Landolfi, A., Colella, S., Marullo,
727 S. and Santoleri, R. (2018). Global Distribution of Non-Algal Particles From Ocean Color Data
728 and Implications for Phytoplankton Biomass Detection. *Geophysical Research Letters*, *45*(15),
729 7672-7682.
- 730 16. Beckers, J.M.; Rixen, M. EOF calculations and data filling from incomplete oceanographic
731 datasets. *J. Atmos. Ocean. Technol.* 2003, *20*, 1839–1856.

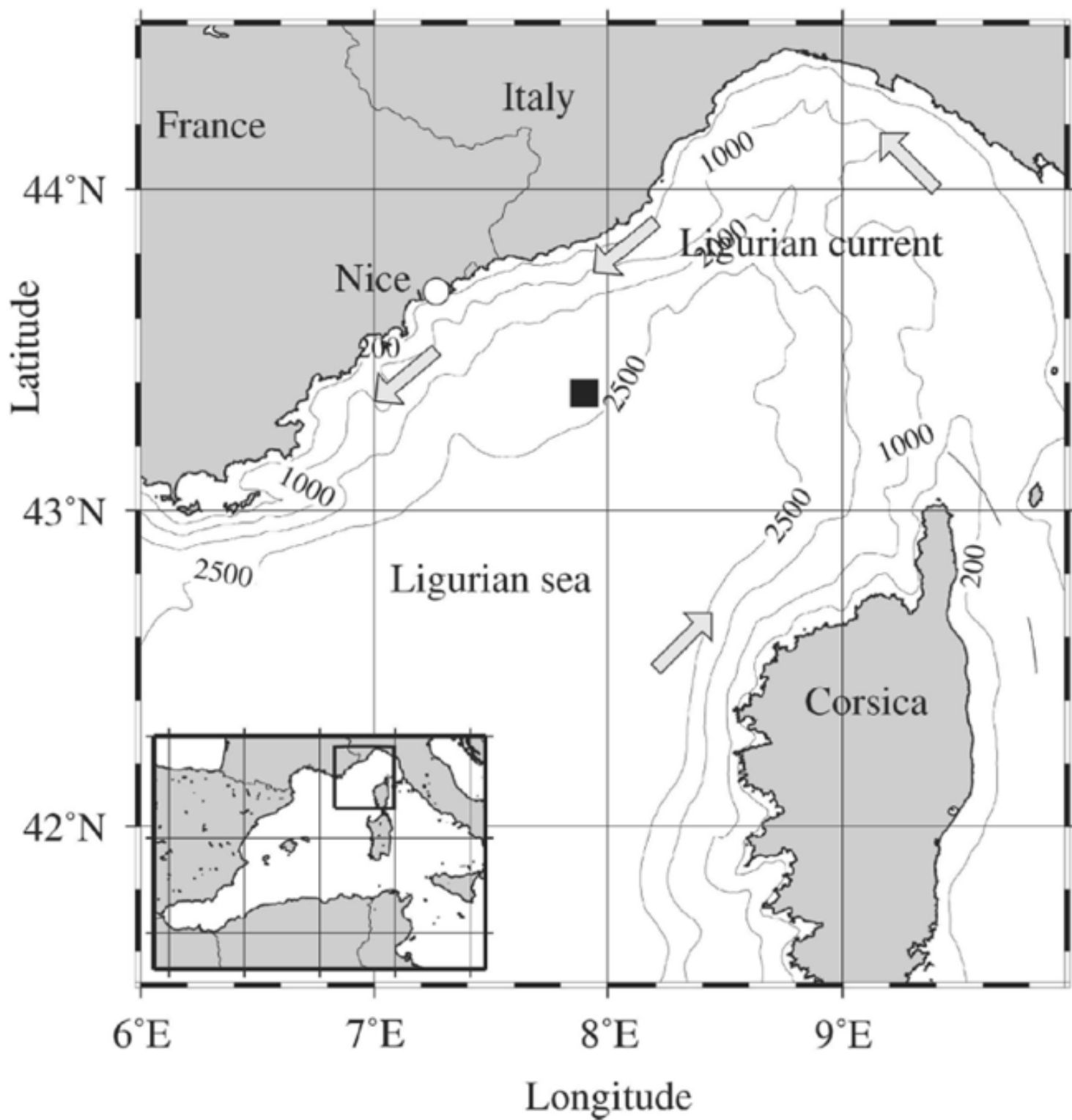
- 732 17. Binder, B. J., & Durand, M. D. (2002). Diel cycles in surface waters of the equatorial
733 Pacific. *Deep Sea Research Part II: Topical Studies in Oceanography*, 49(13), 2601-2617.
- 734 18. Bode, A., Estévez, M. G., Varela, M., & Vilar, J. A. (2015). Annual trend patterns of
735 phytoplankton species abundance belie homogeneous taxonomical group responses to climate in
736 the NE Atlantic upwelling. *Marine environmental research*, 110, 81-91.
- 737 19. Bosc, E., Bricaud, A., & Antoine, D. (2004). Seasonal and interannual variability in algal
738 biomass and primary production in the Mediterranean Sea, as derived from 4 years of SeaWiFS
739 observations. *Global Biogeochemical Cycles*, 18(1).
- 740 20. Boss, E., and W. S. Pegau (2001), Relationship of light scattering at an angle in the backward
741 direction to the backscattering coefficient, *Appl. Opt.*, 40, 5503–5507,
742 doi:10.1364/ao.40.005503.
- 743 21. Brewin, R. J., Dall’Olmo, G., Sathyendranath, S., & Hardman-Mountford, N. J. (2012). Particle
744 backscattering as a function of chlorophyll and phytoplankton size structure in the open-
745 ocean. *Optics express*, 20(16), 17632-17652.
- 746 22. Bricaud, A., Morel, A., & Prieur, L. (1981). Absorption by dissolved organic matter of the sea
747 (yellow substance) in the UV and visible domains. *Limnology and oceanography*, 26(1), 43-53
- 748 23. Carey, C. C., Hanson, P. C., Lathrop, R. C., & St. Amand, A. L. (2016). Using wavelet analyses
749 to examine variability in phytoplankton seasonal succession and annual periodicity. *Journal of*
750 *Plankton Research*, 38(1), 27-40
- 751 24. Cazelles, B., Chavez, M., Berteaux, D., Ménard, F., Vik, J. O., Jenouvrier, S., & Stenseth, N. C.
752 (2008). Wavelet analysis of ecological time series. *Oecologia*, 156(2), 287-304.
- 753 25. Chatfield JR (1989) The analysis of time series: an introduction. Chapman & Hall, London
- 754 26. Claustre, H., A. Morel, M. Babin, C. Cailliau, D. Marie, J. C. Marty, D. Tailliez, and D. Vaultot
755 (1999), Variability in particle attenuation and chlorophyll fluorescence in the tropical Pacific:
756 Scales, patterns, and biogeochemical implications, *J. Geophys. Res.*, 104, 3401–3422, doi:
757 10.1029/98JC01334.
- 758 27. Claustre, H., Bricaud, A., Babin, M., Bruyant, F., Guillou, L., Le Gall, F., ... & Partensky, F.
759 (2002). Diel variations in Prochlorococcus optical properties. *Limnology and*
760 *Oceanography*, 47(6), 1637-1647.
- 761 28. Cleland, E. E., Chuine, I., Menzel, A., Mooney, H. A. & Schwartz, M. D. (2007). Shifting plant
762 phenology in response to climate change. *Trends Ecol. Evol.* 22, 357–365.
- 763 29. Corredor-Acosta, A., Morales, C. E., Hormazabal, S., Andrade, I., & Correa-Ramirez, M. A.
764 (2015). Phytoplankton phenology in the coastal upwelling region off central-southern Chile (35°
765 S–38° S): Time-space variability, coupling to environmental factors, and sources of uncertainty
766 in the estimates. *Journal of Geophysical Research: Oceans*, 120(2), 813-831.
- 767 30. Dall’Olmo, G., Westberry, T. K., Behrenfeld, M. J., Boss, E., & Slade, W. H. (2009).
768 Significant contribution of large particles to optical backscattering in the open
769 ocean. *Biogeosciences*, 6(6), 947-967.
- 770 31. Dall’Olmo, G., Boss, E., Behrenfeld, M. J., & Westberry, T. K. (2012). Particulate optical
771 scattering coefficients along an Atlantic Meridional Transect. *Optics express*, 20(19), 21532-
772 21551. Damarcq, H., Reygondeau, G., Alvain, S., & Vantrepotte, V. (2012). Monitoring marine
773 phytoplankton seasonality from space. *Remote Sensing of Environment*, 117, 211-222.
- 774 32. Daubechies, I. (1992). Ten lectures on wavelets. Society for industrial and applied mathematics.
- 775 33. D’Ortenzio, F., Iudicone, D., de Boyer Montegut, C., Testor, P., Antoine, D., Marullo, S., ... &
776 Madec, G. (2005). Seasonal variability of the mixed layer depth in the Mediterranean Sea as
777 derived from in situ profiles. *Geophysical Research Letters*, 32(12).
- 778 34. D’Ortenzio, F., Lavigne, H., Besson, F., Claustre, H., Coppola, L., Garcia, N., ... & Morin, P.
779 (2014). Observing mixed layer depth, nitrate and chlorophyll concentrations in the northwestern
780 Mediterranean: A combined satellite and NO₃ profiling floats experiment. *Geophysical*
781 *Research Letters*, 41(18), 6443-6451

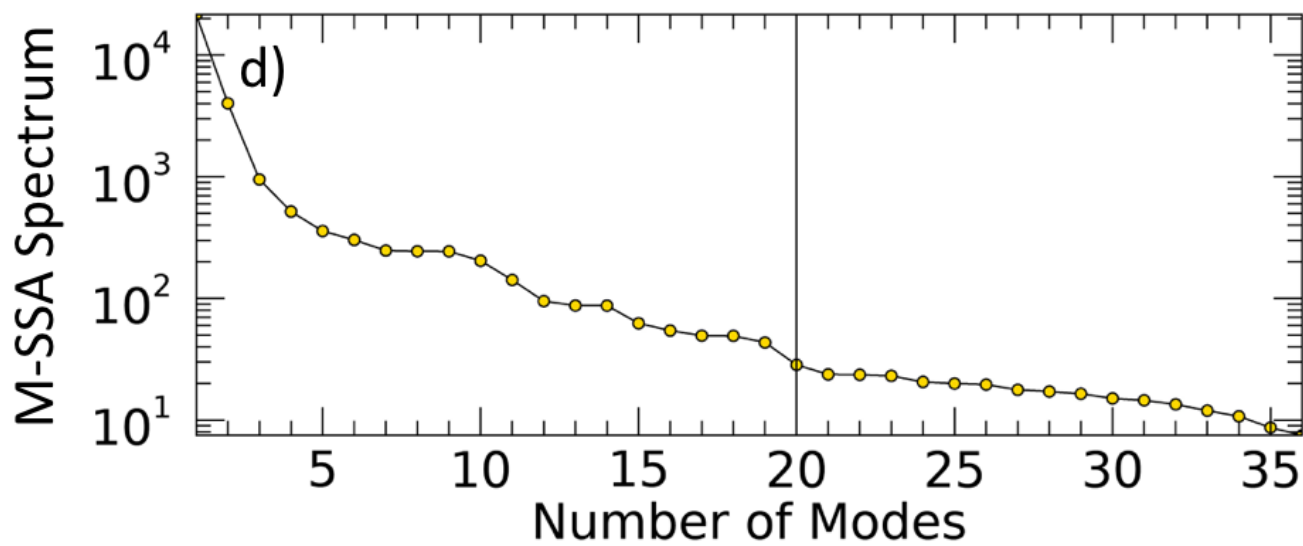
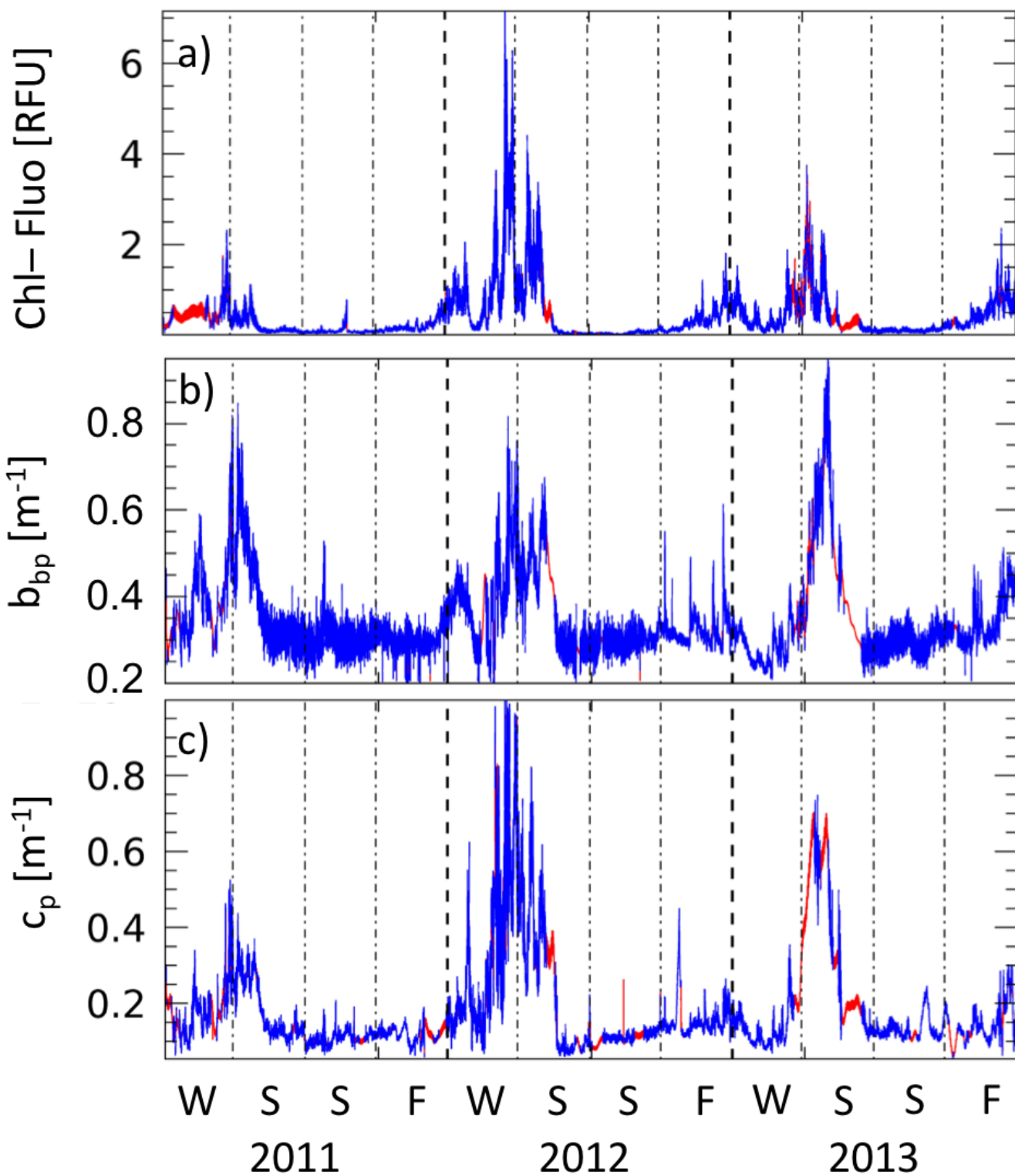
- 782 35. Durand, M. D., & Olson, R. J. (1998). Diel patterns in optical properties of the chlorophyte
783 *Nannochloris* sp.: Relating individual-cell to bulk measurements. *Limnology and*
784 *Oceanography*, 43(6), 1107-1118.
- 785 36. García-Reyes, M., Sydeman, W. J., Black, B. A., Rykaczewski, R. R., Schoeman, D. S.,
786 Thompson, S. A., & Bograd, S. J. (2013). Relative influence of oceanic and terrestrial pressure
787 systems in driving upwelling-favorable winds. *Geophysical Research Letters*, 40(19), 5311-
788 5315.
- 789 37. Gernez, P., Antoine, D., & Huot, Y. (2011). Diel cycles of the particulate beam attenuation
790 coefficient under varying trophic conditions in the northwestern Mediterranean Sea:
791 Observations and modeling. *Limnology and Oceanography*, 56(1), 17-36.
- 792 38. Ghil, M., Allen, M. R., Dettinger, M. D., Ide, K., Kondrashov, D., Mann, M. E., ... & Yiou, P.
793 (2002). Advanced spectral methods for climatic time series. *Reviews of geophysics*, 40(1)
- 794 39. Halsey, K. H., & Jones, B. M. (2015). Phytoplankton strategies for photosynthetic energy
795 allocation. *Annual review of marine science*, 7, 265-297.
- 796 40. Huot, Y., Babin, M., Bruyant, F., Grob, C., Twardowski, M., Claustre, H., 2007. Relationship
797 between photosynthetic parameters and different proxies of phytoplankton biomass in the
798 subtropical ocean. *Biogeosciences*, 4 (5), 853–868.
- 799 41. Huot, Y., Morel, A., Twardowski, M.S., Stramski, D., Reynolds, R.A., 2008. Particle optical
800 backscattering along a chlorophyll gradient in the upper layer of the eastern South Pacific
801 Ocean. *Biogeosciences*, 5 (2), 495–507.
- 802 42. Ji, R., Edwards, M., Mackas, D. L., Runge, J. A., & Thomas, A. C. (2010). Marine plankton
803 phenology and life history in a changing climate: current research and future directions. *Journal*
804 *of plankton research*, 32(10), 1355-1368.
- 805 43. Kheireddine, M., & Antoine, D. (2014). Diel variability of the beam attenuation and
806 backscattering coefficients in the northwestern Mediterranean Sea (BOUSSOLE site). *Journal*
807 *of Geophysical Research: Oceans*, 119(8), 5465-5482
- 808 44. Kondrashov, D., Feliks, Y., & Ghil, M. (2005). Oscillatory modes of extended Nile River
809 records (AD 622–1922). *Geophysical research letters*, 32(10).
- 810 45. Kondrashov, D., & Ghil, M. (2006). Spatio-temporal filling of missing points in geophysical
811 data sets. *Nonlinear Processes in Geophysics*, 13(2), 151-159.
- 812 46. Kondrashov, D., Shpirts, Y., & Ghil, M. (2010). Gap filling of solar wind data by singular
813 spectrum analysis. *Geophysical research letters*, 37(15) Lavigne, H., D'Ortenzio, F., Migon, C.,
814 Claustre, H., Testor, P., d'Alcalà, M. R., ... & Prieur, L. (2013). Enhancing the comprehension
815 of mixed layer depth control on the Mediterranean phytoplankton phenology. *Journal of*
816 *Geophysical Research: Oceans*, 118(7), 3416-3430.
- 817 47. Lau KM, Weng H (1995). Climatic signal detection using wavelet transform: how to make a
818 time series sing. *Bull Am Meteorol Soc* 76:2391–2402
- 819 48. Lee, Z. P., K. L. Carder, and R. A. Arnone (2002), Deriving inherent optical properties from
820 water color: A multiband quasi-analytical algorithm for optically deep waters, *Appl. Opt.*, 41,
821 5755–5772, doi:10.1364/ao.41.005755.
- 822 49. Loisel, H., Bosc, E., Stramski, D., Oubelkheir, K., & Deschamps, P. Y. (2001). Seasonal
823 variability of the backscattering coefficient in the Mediterranean Sea based on satellite
824 SeaWiFS imagery. *Geophysical Research Letters*, 28(22), 4203-4206.
- 825 50. Loisel, H., Vantrepotte, V., Norkvist, K., Meriaux, X., Kheireddine, M., Ras, J., ... & Mauriac,
826 R. (2011). Characterization of the bio-optical anomaly and diurnal variability of particulate
827 matter, as seen from scattering and backscattering coefficients, in ultra-oligotrophic eddies of
828 the Mediterranean Sea. *Biogeosciences*, 8(11), 3295-3317.
- 829 51. Maffione, R. A., and D. R. Dana (1997), Instruments and methods for measuring the backward-
830 scattering coefficient of ocean waters, *Appl. Opt.*, 36, 6057–6067, doi:10.1364/ao.36.006057.

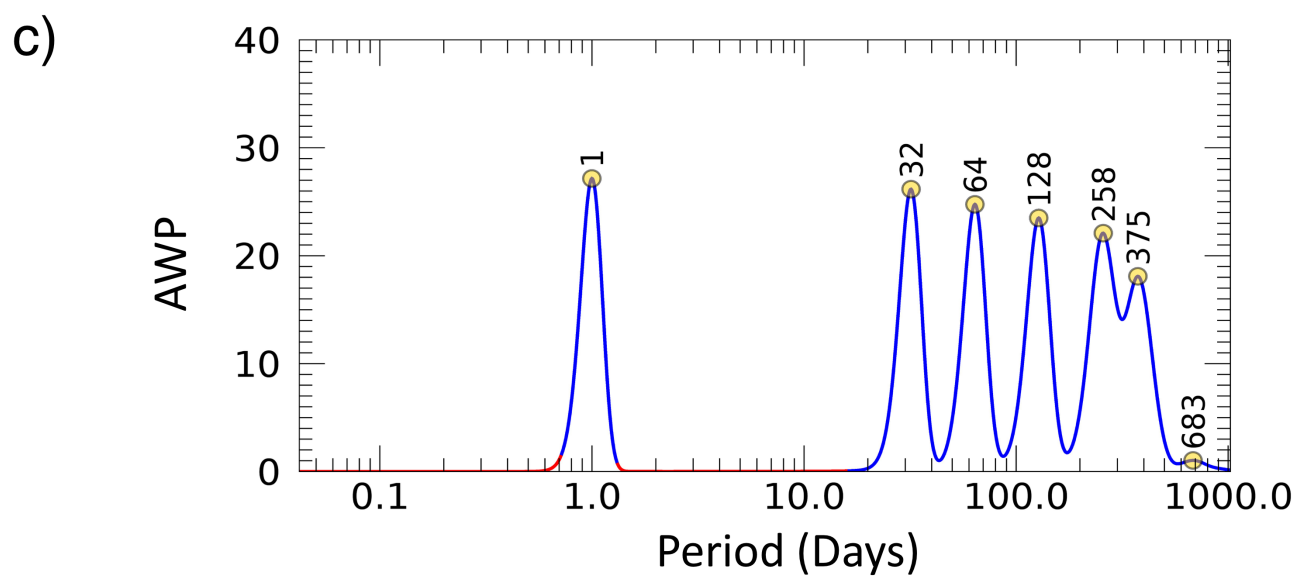
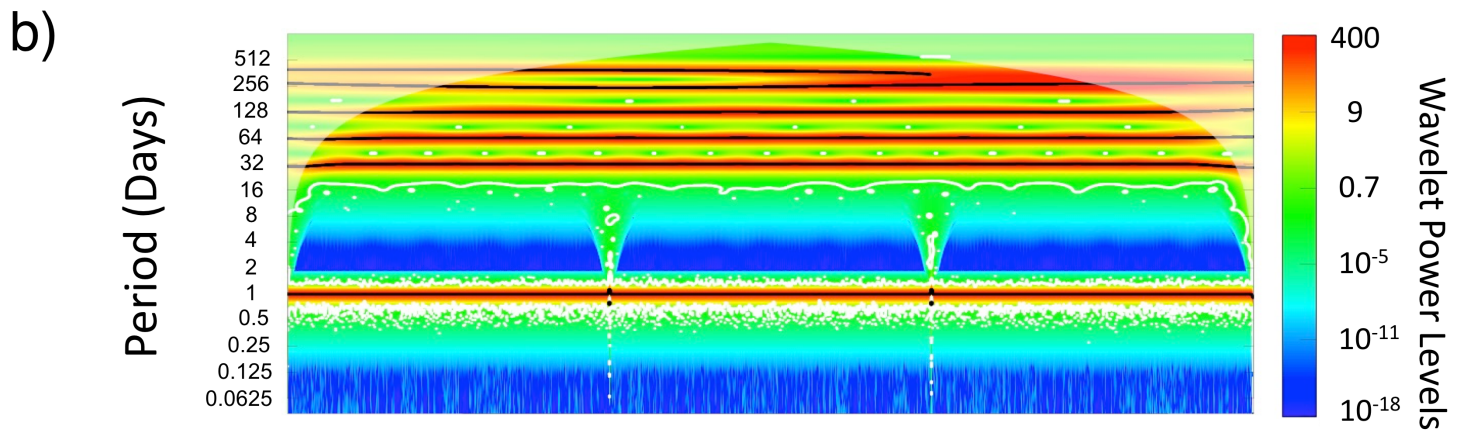
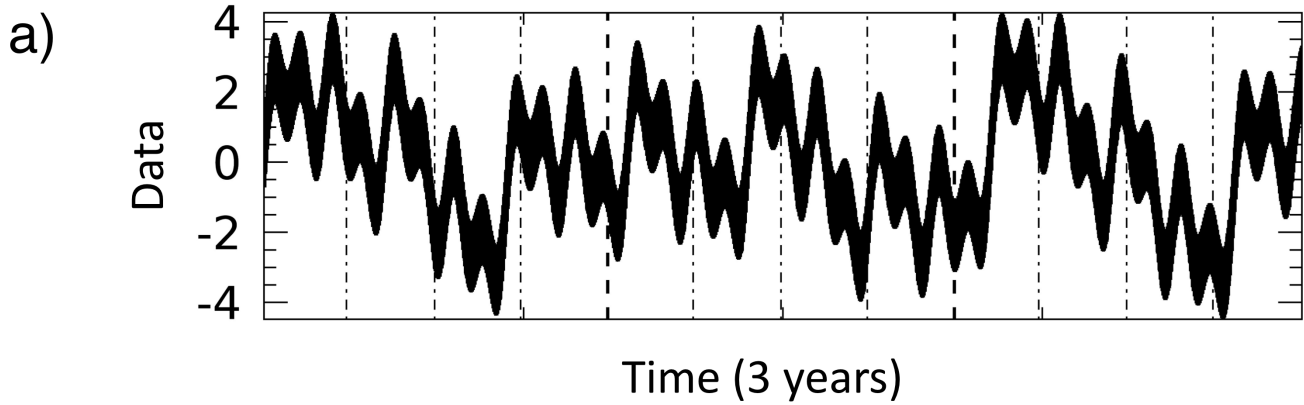
- 831 52. Martinez-Vicente, V., Dall'Olmo, G., Tarran, G., Boss, E., & Sathyendranath, S. (2013). Optical
832 backscattering is correlated with phytoplankton carbon across the Atlantic Ocean. *Geophysical*
833 *Research Letters*, 40(6), 1154-1158.
- 834 53. Mayot, N., D'Ortenzio, F., d'Alcala, M. R., Lavigne, H., & Claustre, H. (2016). Interannual
835 variability of the Mediterranean trophic regimes from ocean color
836 satellites. *Biogeosciences*, 13(6), 1901-1917.
- 837 54. Mayot, N., D'Ortenzio, F., Uitz, J., Gentili, B., Ras, J., Vellucci, V., ... & Claustre, H. (2017).
838 Influence of the phytoplankton community structure on the spring and annual primary
839 production in the North-Western Mediterranean Sea. *Journal of Geophysical Research: Oceans*.
- 840 55. Mignot, A., Claustre, H., Uitz, J., Poteau, A., D'Ortenzio, F., & Xing, X. (2014). Understanding
841 the seasonal dynamics of phytoplankton biomass and the deep chlorophyll maximum in
842 oligotrophic environments: A Bio-Argo float investigation. *Global Biogeochemical*
843 *Cycles*, 28(8), 856-876
- 844 56. Mignot, A., Ferrari, R., & Claustre, H. (2018). Floats with bio-optical sensors reveal what
845 processes trigger the North Atlantic bloom. *Nature Communications*, 9(1), 190.
- 846 57. Millot, C. (1999). Circulation in the western Mediterranean Sea. *Journal of marine*
847 *systems*, 20(1), 423-442.
- 848 58. Monteiro, P., Gregor, L., Lévy, M., Maenner, S., Sabine, C. L., & Swart, S. (2015).
849 Intraseasonal variability linked to sampling alias in air-sea CO₂ fluxes in the Southern
850 Ocean. *Geophysical Research Letters*, 42(20), 8507-8514.
- 851 59. Morel, A., and Y.-H. Ahn (1991), Optics of heterotrophic nanoflagellates and ciliates: A
852 tentative assessment of their scattering role in oceanic waters compared to those of bacterial and
853 algal cells, *Journal of Marine Research*, 49, 177–202.
- 854 60. Morlet J., Arens G., Fourgeau E., and Giard D., 1982. Wave propagation and sampling theory –
855 Part I: complex signal and scattering in multilayered media. *Geophysics*, 47, 203–221.
- 856 61. Morlet J., Arens G., Fourgeau E., and Giard D., 1982. Wave propagation and sampling theory –
857 Part II: sampling theory and complex waves. *Geophysics*, 47, 222–236.
- 858 62. Morren C (1849a) Le Globe, le Temps et la Vie. *Bulletins de l'Académie royale des Sciences,*
859 *des Lettres et des Beaux-Arts de Belgique*, XVI(2):660–684
- 860 63. Neukermans, G., Loisel, H., Mériaux, X., Astoreca, R., & McKee, D. (2012). In situ variability
861 of mass-specific beam attenuation and backscattering of marine particles with respect to particle
862 size, density, and composition. *Limnology and Oceanography*, 57(1), 124-144.
- 863 64. Neveux, J.; Dupouy, C.; Blanchot, J.; Le Bouteiller, A.; Landry, M.R.; Brown, S.L. Diel
864 dynamics of chlorophylls in high-nutrient, low-chlorophyll waters of the equatorial Pacific
865 (180°). (2003) Interactions of growth, grazing, physiological responses, and mixing. *J. Geophys.*
866 *Res. Oceans*, 108, doi:10.1029/2000JC000747.
- 867 65. Nezlin, N. P., Afanasyev, Y. D., Ginzburg, A. I., & Kostianoy, A. G. (2002). Remotely sensed
868 studies of phytoplankton dynamics under physical forcing in different ocean regions. *Advances*
869 *in Space Research*, 29(1), 99-106.
- 870 66. Organelli, E., Dall'Olmo, G., Brewin, R. J., Tarran, G. A., Boss, E., & Bricaud, A. (2018). The
871 open-ocean missing backscattering is in the structural complexity of particles. *Nature*
872 *communications*, 9(1), 5439.
- 873 67. Oubelkheir, K., Claustre, H., Sciandra, A., & Babin, M. (2005). Bio-optical and biogeochemical
874 properties of different trophic regimes in oceanic waters. *Limnology and oceanography*, 50(6),
875 1795-1809.
- 876 68. Oubelkheir, K., & Sciandra, A. (2008). Diel variations in particle stocks in the oligotrophic
877 waters of the Ionian Sea (Mediterranean). *Journal of Marine Systems*, 74(1), 364-371.
- 878 69. Percival, D. B., & Walden, A. T. (2000). Wavelet methods for time series analysis, vol. 4 of
879 Cambridge Series in Statistical and Probabilistic Mathematics.

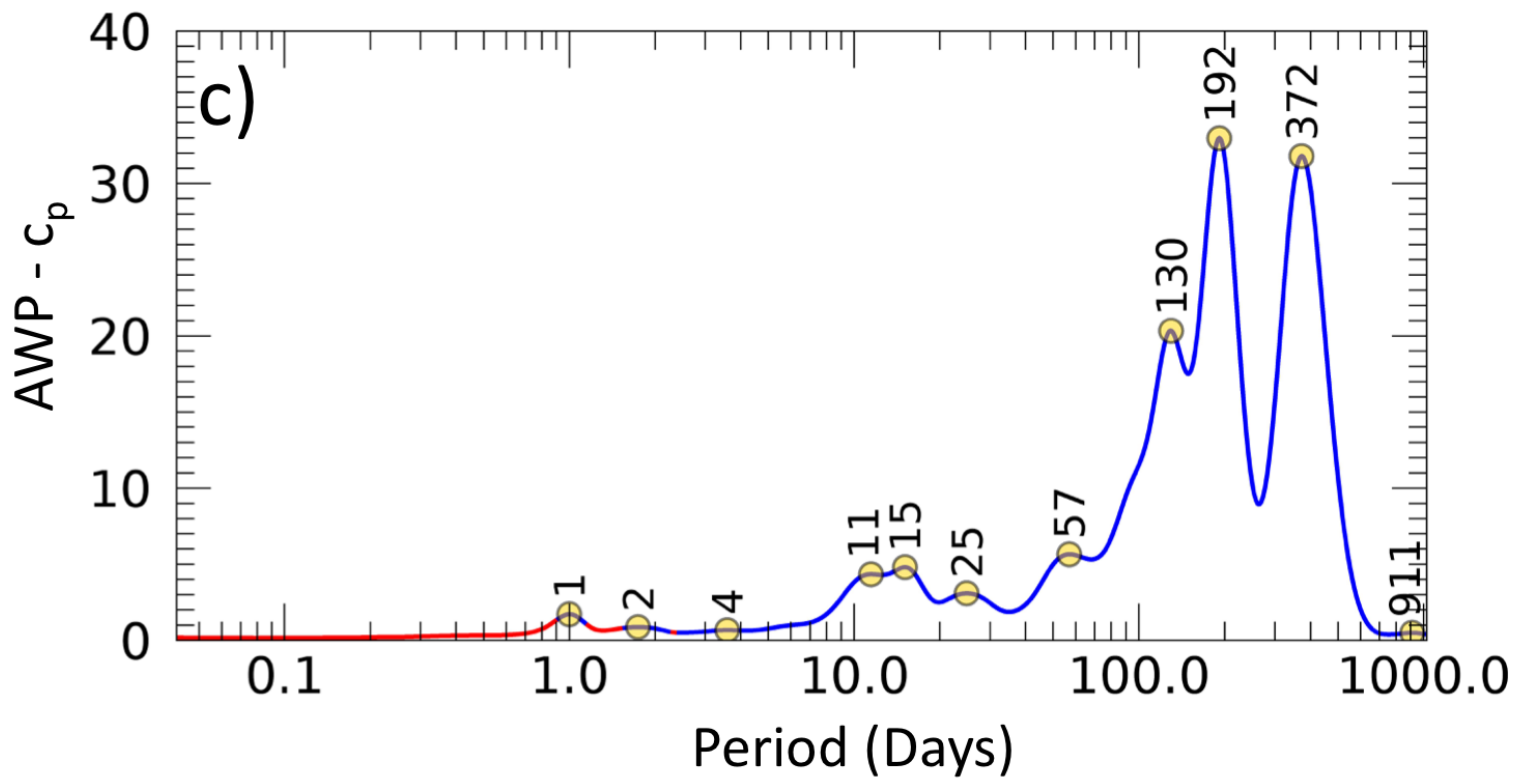
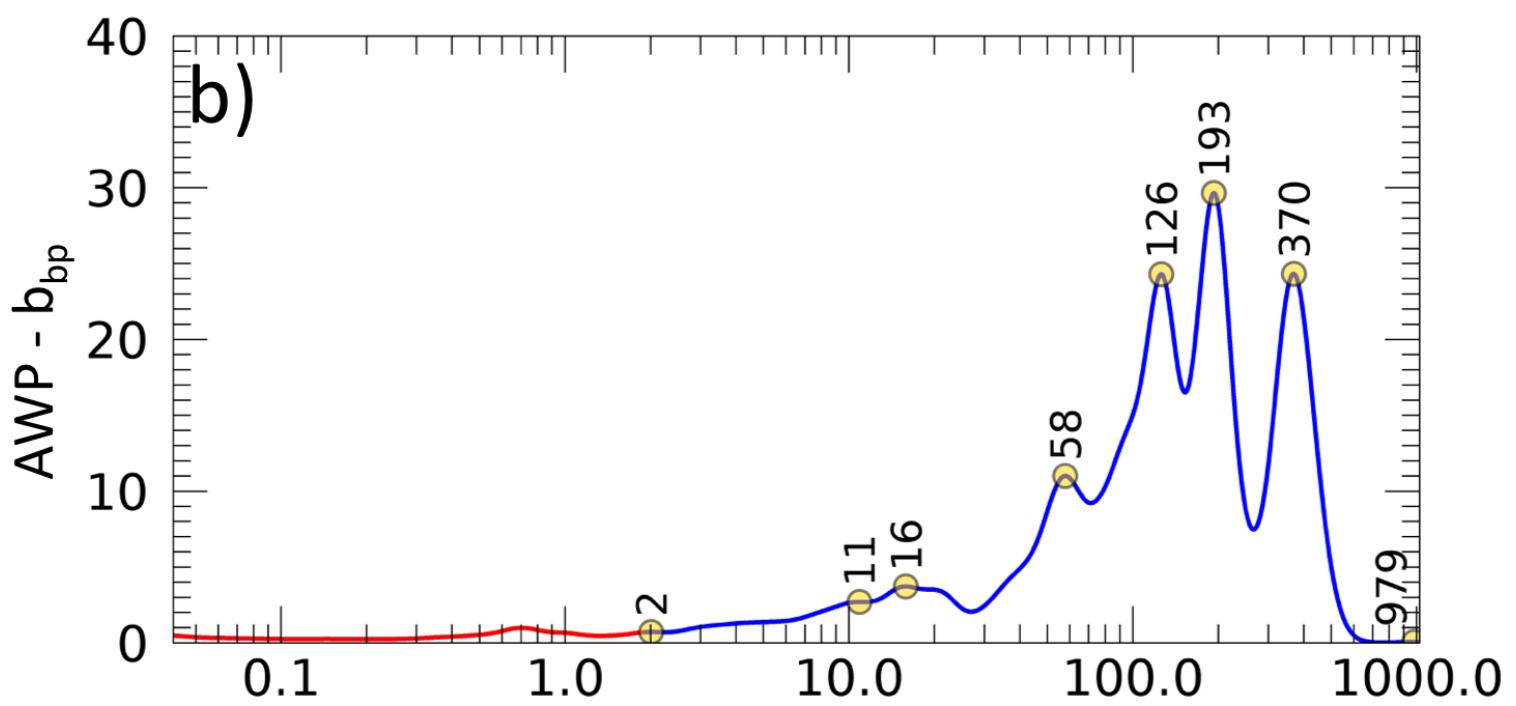
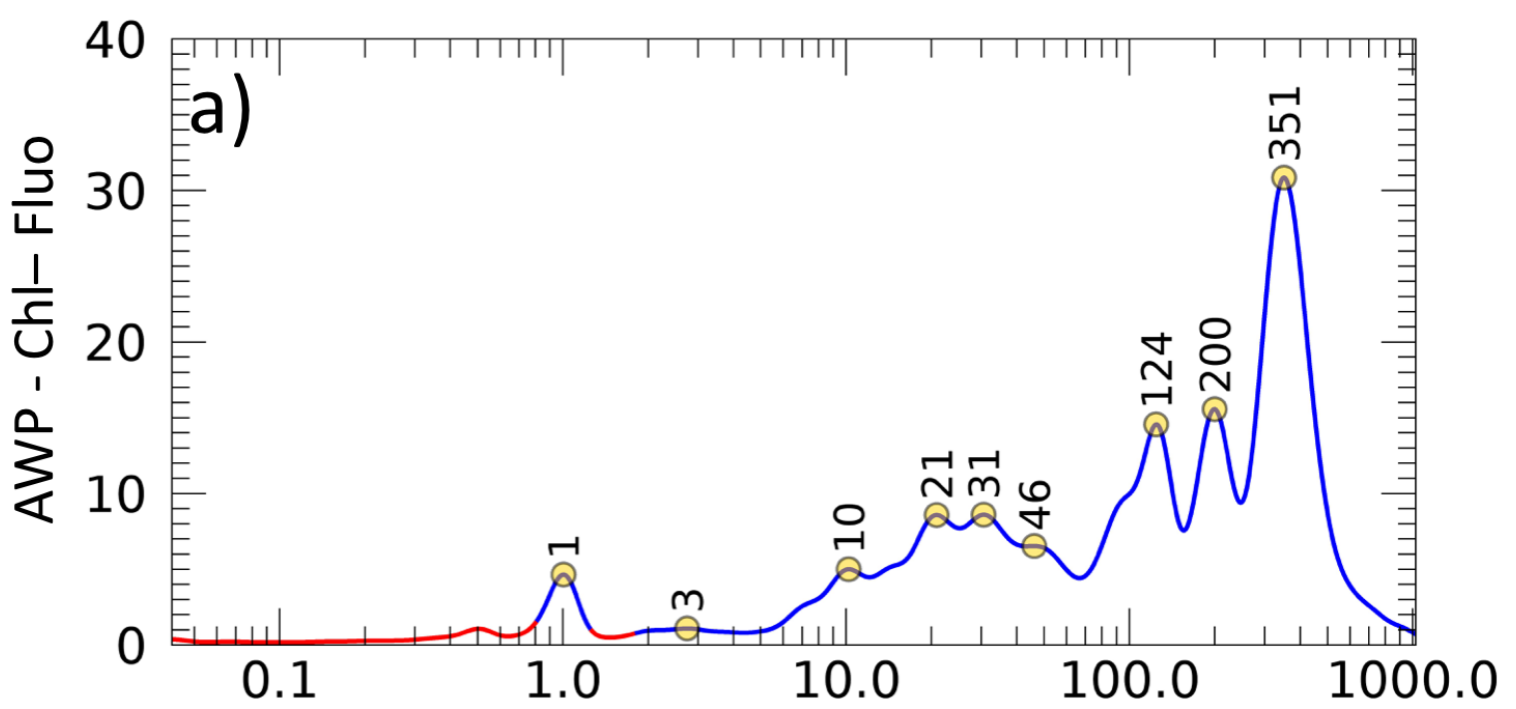
- 880 70. Poulin, C., Antoine, D., & Huot, Y. (2018). Diurnal variations of the optical properties of
881 phytoplankton in a laboratory experiment and their implication for using inherent optical
882 properties to measure biomass. *Optics Express*, 26(2), 711-729
- 883 71. Roesch, A., & Schmidbauer, H. (2014). WaveletComp: Computational Wavelet Analysis. R
884 package version 1.0.
- 885 72. Sala, I., Navarro, G., Bolado-Penagos, M., Echevarría, F., & García, C. M. (2018). High-
886 Chlorophyll-Area Assessment Based on Remote Sensing Observations: The Case Study of Cape
887 Trafalgar. *Remote Sensing*, 10(2), 165.
- 888 73. Sammartino, M., Di Cicco, A., Marullo, S., & Santoleri, R. (2015). Spatio-temporal variability
889 of micro-, nano-and pico-phytoplankton in the Mediterranean Sea from satellite ocean colour
890 data of SeaWiFS. *Ocean Science*, 11(5), 759.
- 891 74. Siegel, D. A., T. D. Dickey, L. Washburn, M. K. Hamilton, and B. G. Mitchell (1989), Optical
892 determination of particulate abundance and production variations in the oligotrophic ocean,
893 *Deep Sea Res., Part A*, 36, 211–222, doi:10.1016/0198-0149(89)90134-9.
- 894 75. Siegel, D. A., Behrenfeld, M. J., Maritorena, S., McClain, C. R., Antoine, D., Bailey, S. W., ...
895 & Eplee Jr, R. E. (2013). Regional to global assessments of phytoplankton dynamics from the
896 SeaWiFS mission. *Remote Sensing of Environment*, 135, 77-91.
- 897 76. Slade, W. H., & Boss, E. (2015). Spectral attenuation and backscattering as indicators of
898 average particle size. *Applied optics*, 54(24), 7264-7277.
- 899 77. Sosik, H. M. (2008). Characterizing seawater constituents from optical properties. In M. Babin,
900 C. S. Roesler, & J. J. Cullen (Eds.), *Real-time coastal observing systems for ecosystem
901 dynamics and harmful algal blooms* (pp. 281–329). Paris, France: UNESCO. (peer reviewed)
- 902 78. Stramski, D., and D. A. Kiefer (1991), Light scattering by microorganisms in the open ocean,
903 *Prog. Oceanogr.*, 28, 343–383, doi:10.1016/0079-6611(91)90032-h.
- 904 79. Stramski, D., and R. A. Reynolds (1993), Diel variations in the optical properties of a marine
905 diatom, *Limnology and Oceanography*, 38, 1347–1364
- 906 80. Stramski, D., Boss, E., Bogucki, D., & Voss, K. J. (2004). The role of seawater constituents in
907 light backscattering in the ocean. *Progress in Oceanography*, 61(1), 27-56.
- 908 81. Stramski, D., A. Shalapyonok, and R. A. Reynolds (1995), Optical characterisation of the
909 oceanic unicellular cyanobacterium *Synechococcus* grown under a day-night cycle in natural
910 irradiance, *J. Geophys. Res.*, 100, 13,295–13,307, doi:10.1029/95jc00452.
- 911 82. Torrence, C., & Compo, G. P. (1998). A practical guide to wavelet analysis. *Bulletin of the
912 American Meteorological society*, 79(1), 61-78.
- 913 83. Twardowski, M. S., Boss, E., Macdonald, J. B., Pegau, W. S., Barnard, A. H., & Zaneveld, J. R.
914 V. (2001). A model for estimating bulk refractive index from the optical backscattering ratio
915 and the implications for understanding particle composition in case I and case II waters. *Journal
916 of Geophysical Research: Oceans*, 106(C7), 14129-14142
- 917 84. Volpe, G., Nardelli, B. B., Cipollini, P., Santoleri, R., & Robinson, I. S. (2012). Seasonal to
918 interannual phytoplankton response to physical processes in the Mediterranean Sea from
919 satellite observations. *Remote Sensing of Environment*, 117, 223-235.
- 920 85. Walsh, I. D., S. P. Chung, M. J. Richardson, and W. D. Gardner (1995), The diel cycle in the
921 integrated particle load in the equatorial pacific: A comparison with primary production, *Deep
922 Sea Res., Part II*, 42, 465–477, doi:10.1016/0967-0645(95)00030-t.
- 923 86. Winder, M., & Cloern, J. E. (2010). The annual cycles of phytoplankton biomass. *Philosophical
924 Transactions of the Royal Society B: Biological Sciences*, 365(1555), 3215-3226.
- 925 87. Xing, X., Claustre, H., Boss, E., Roesler, C., Organelli, E., Poteau, A., ... & D'Ortenzio, F.
926 (2017). Correction of profiles of in-situ chlorophyll fluorometry for the contribution of
927 fluorescence originating from non-algal matter. *Limnology and Oceanography: Methods*, 15(1),
928 80-93
- 929 88. Zhang, X. D., and L. B. Hu (2009), Estimating scattering of pure water from density fluctuation
930 of the refractive index, *Opt. Express*, 17, 1671–1678.

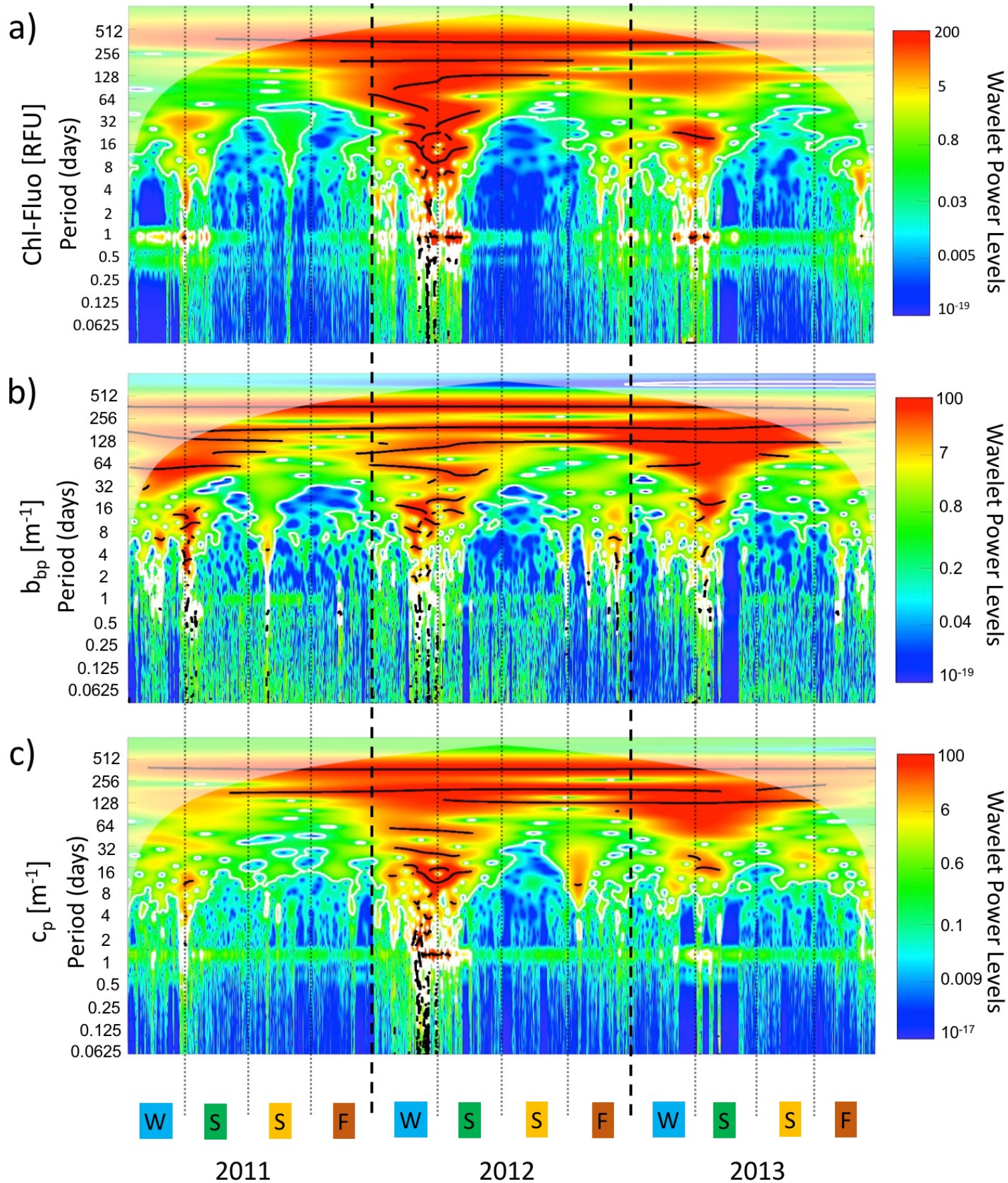
931 89. Zhang, X. D., L. B. Hu, and M. X. He (2009), Scattering by pure seawater: Effect of salinity,
932 *Opt. Express*, 17, 5698–5710.

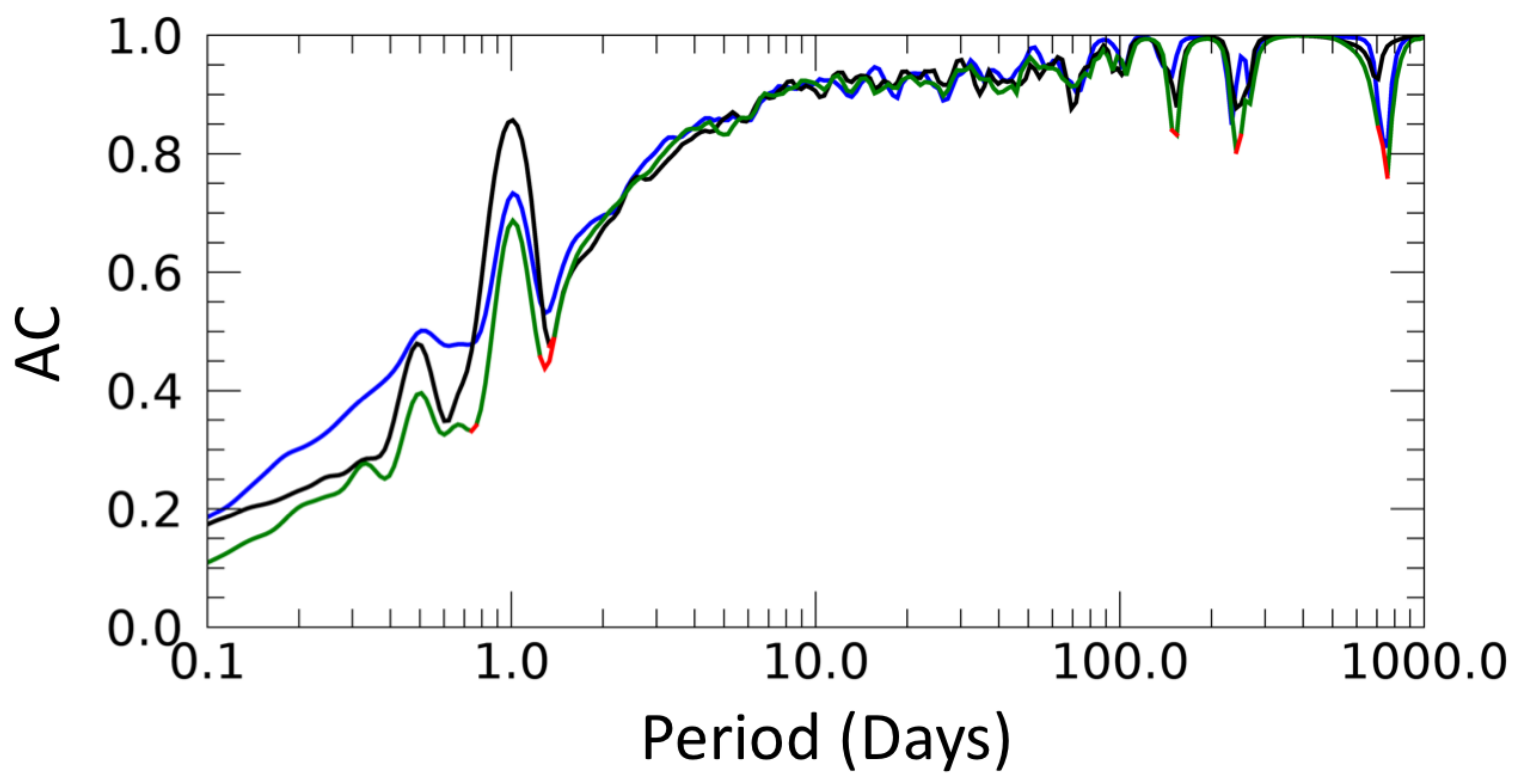


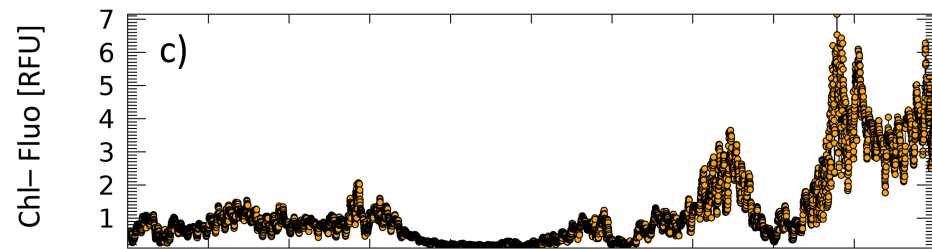
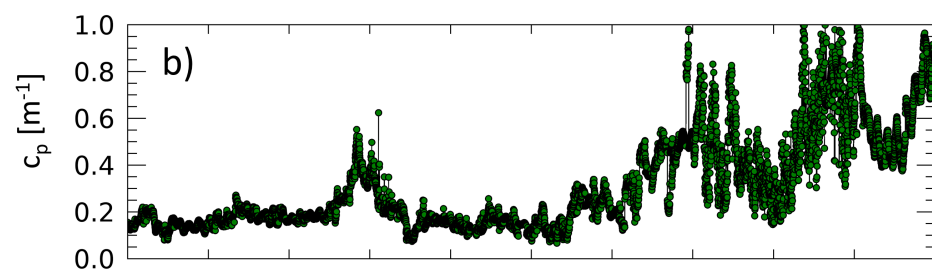
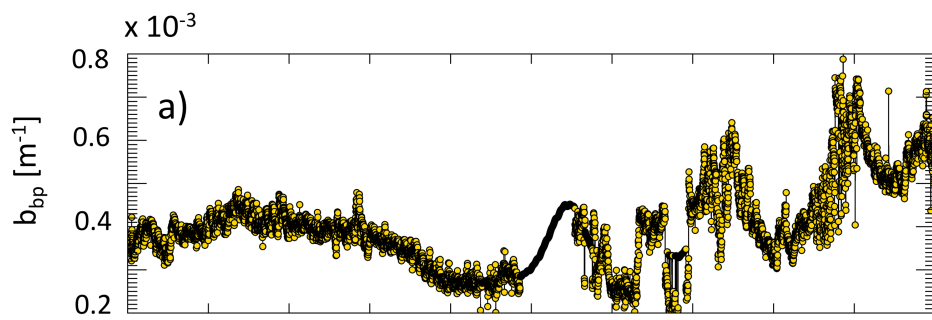




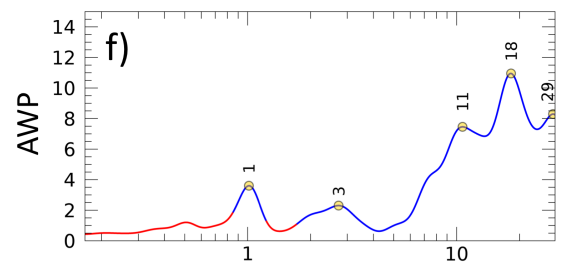
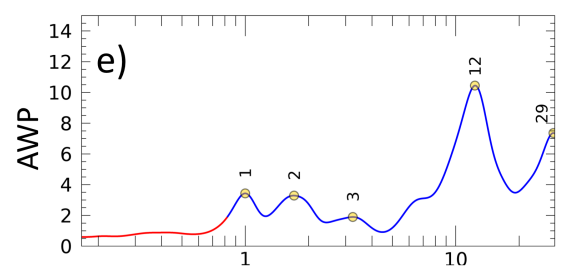
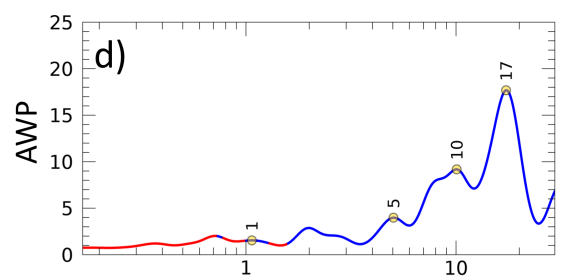




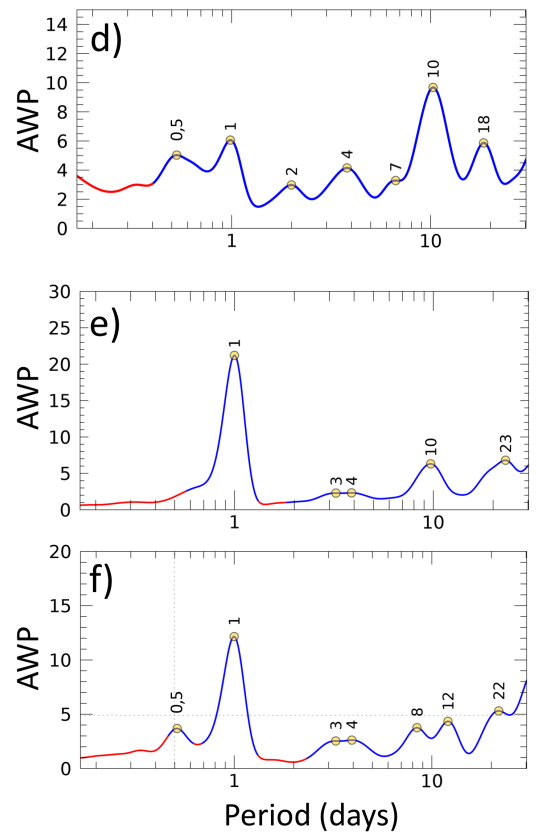
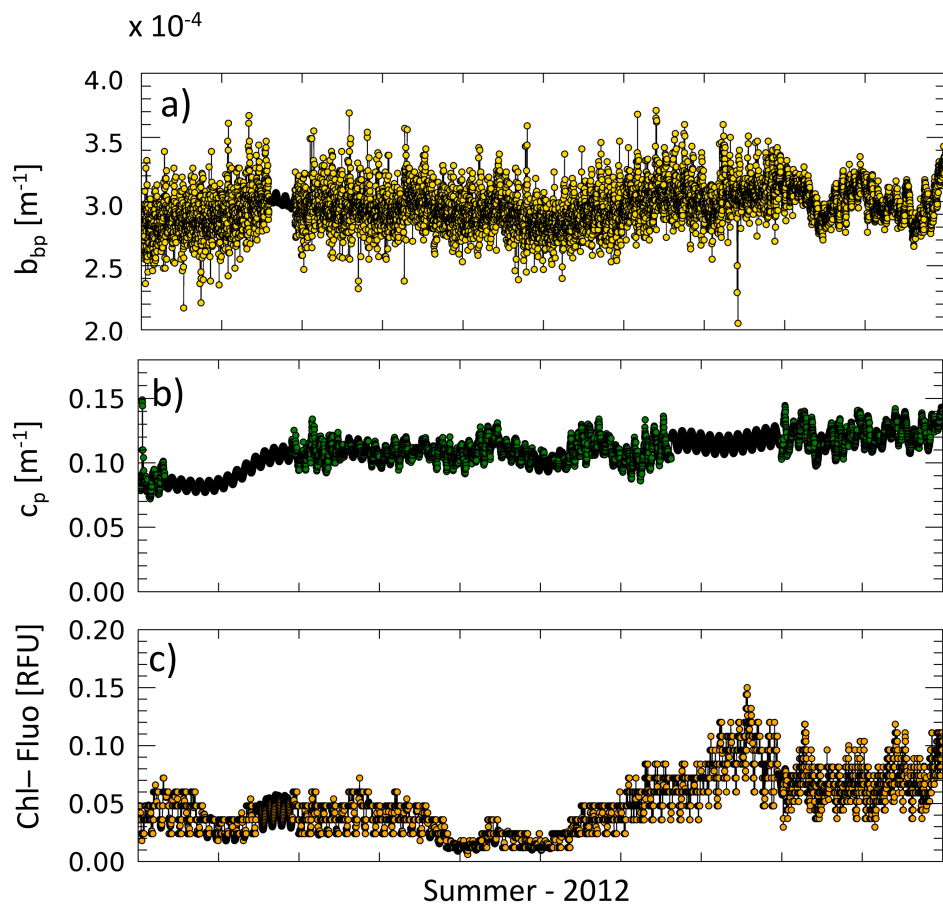


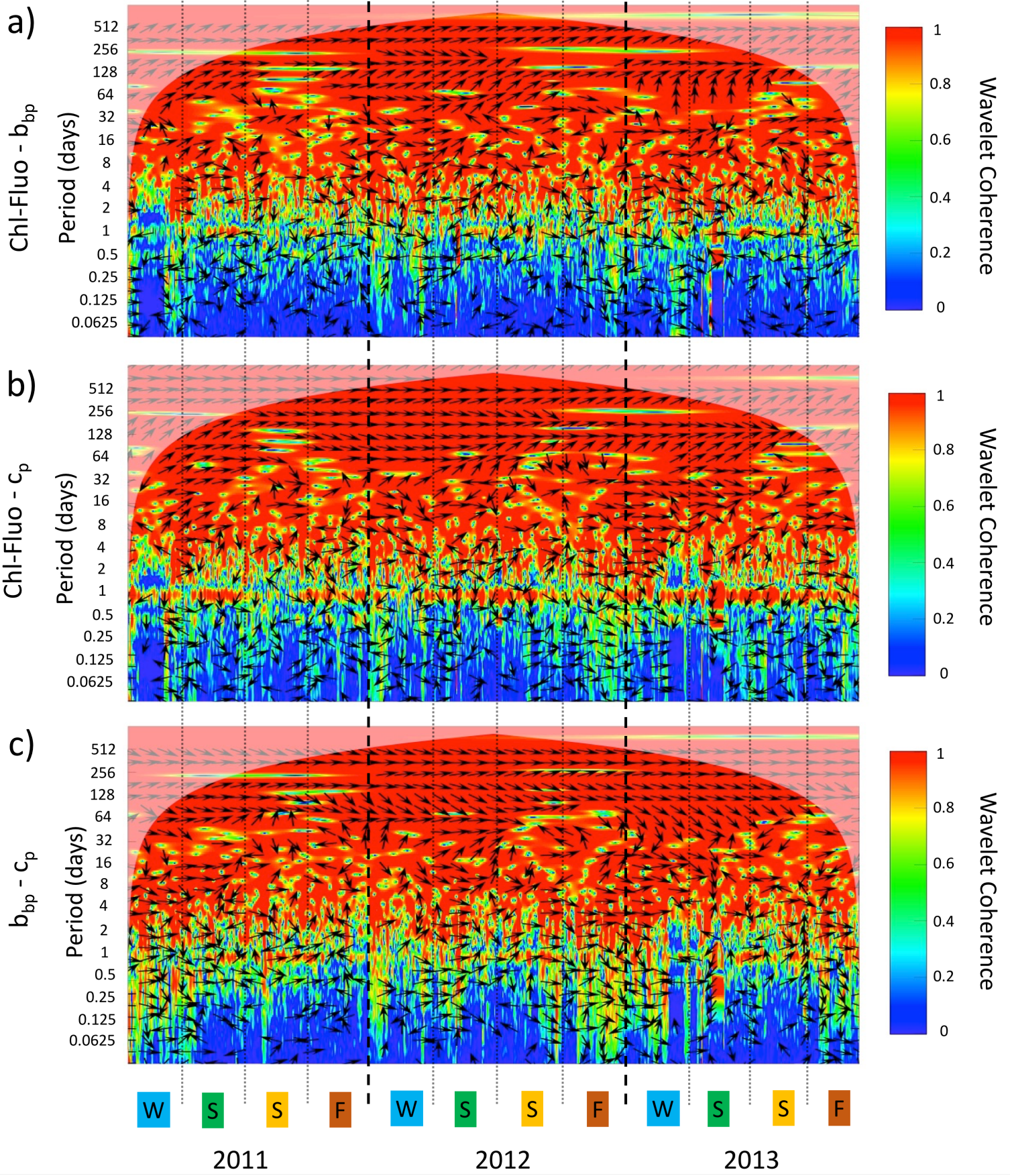


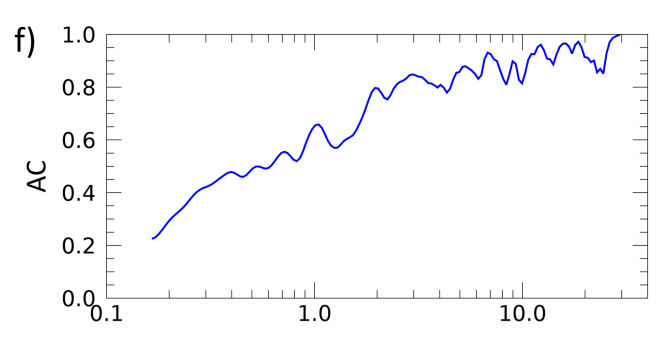
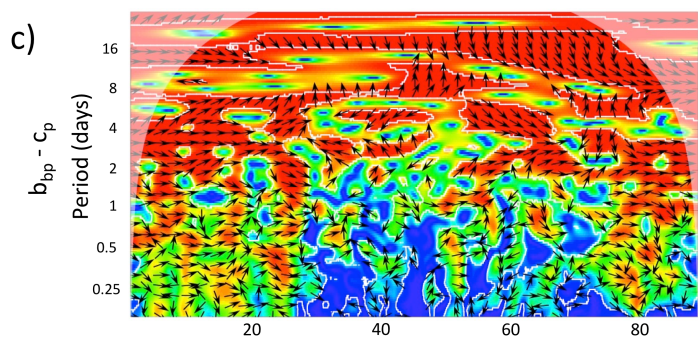
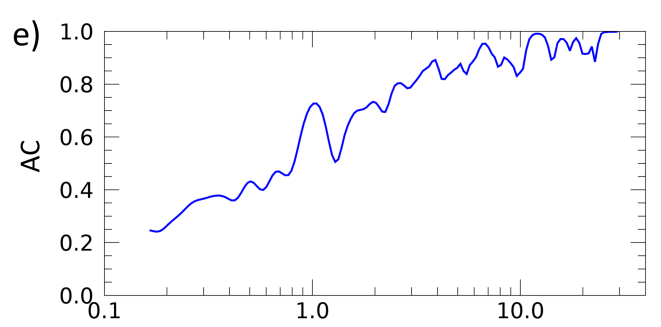
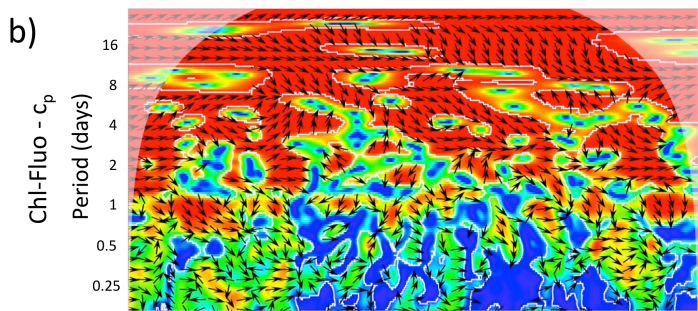
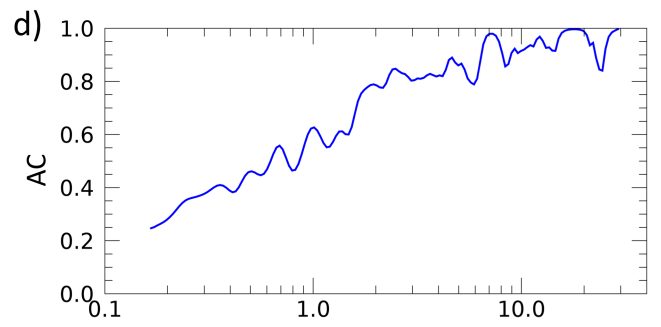
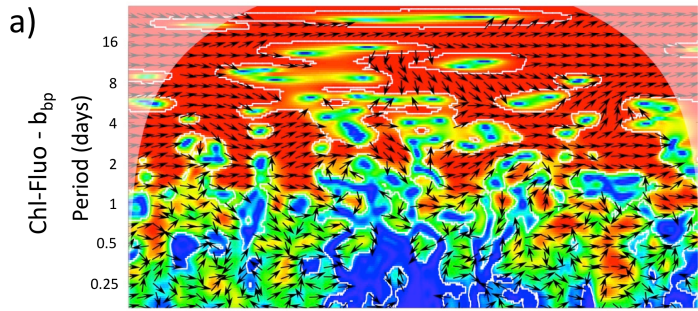
Winter - 2012



Period (days)







Winter 2012 (days)

Period (days)

